



NAM

**Advanced modelling of URM buildings in support
of fragility and consequence functions derivation
Using the Applied Element Method to
model the shake-table testing of two full-
scale URM houses**

Daniele Malomo and Rui Pinho

Mosayk

Date October 2017

Editors Jan van Elk & Dirk Doornhof

General Introduction

Many of the buildings in the Groningen field area are terraced unreinforced masonry buildings. A program to assess the response of these building to earthquakes was therefore initiated. This program built on the experimental and modelling program into the properties of URM building materials, wall elements and wall units.

A typical Groningen terraced house built using materials from the Groningen area by builders from the Groningen area, was tested at the shake-table of Eucentre in Pavia, Italy (Ref. 1). Although the building was at the end of this test program seriously damaged, the building had not collapsed. This left questions on the remaining capacity of the structure and its ability to resist larger seismic movements before (partially) collapsing. The test in Eucentre was therefore followed-up with further tests at the laboratory of LNEC in Lisbon, Portugal (Ref. 2 to 5). Here the upper floors of the building tested in Eucentre were re-built in the LNEC laboratory and subjected to movements measured at the base of the upper floors in Eucentre.

Additionally, detached terraced unreinforced masonry building was built in the Eucentre laboratory and was tested at the shake-table (Ref. 6 and 7). Also this building was constructed using materials from the Groningen area by builders from the Groningen area.

This report shows the results of modelling of these two shake-table testing programs obtained by Mosayk using Extreme Loading for Structures (ELS), a commercial structural analysis software based on the Applied Element Method (AEM) after such tests, describing also the calibration process of the AEM numerical model.

References

1. Eucentre Shake-table Test of Terraced House Modelling Predictions and Analysis Cross Validation, staff from ARUP, Eucentre (Pavia) and TU Delft, November 2015 [this document also includes; (1) Instruments full-scale test-house Eucentre Laboratory, (2) Protocol for Shaking Table Test on Full Scale Building (Eucentre) V_1, and (3) Selection of Acceleration Time-Series for Shake Table Testing of Groningen Masonry Building at the EUCENTRE, Pavia, all three by staff from Eucentre (Pavia)],
2. Collapse shake-table testing of terraced house (LNEC-BUILD1), Eucentre and LNEC (U. Tomassetti, A. A. Correia, F. Graziotti, A.I. Marques, M. Mandirola, P.X. Candeias), 1st September 2017.
3. Using the Applied Element Method to model the collapse shake-table testing of a URM cavity wall structure (LNEC-BUILD1), Mosayk (D. Malomo, R. Pinho), 31st October 2017.
4. Shake-table test up to collapse on a roof substructure of a Dutch terraced house (LNEC-BUILD2), Eucentre and LNEC (A.A. Correia, A.I. Marques, V. Bernardo, L. Grottoli, U. Tomassetti, F. Graziotti), 31st October 2017.
5. Using the Applied Element Method to model the collapse shake-table testing of a terraced house roof substructure (LNEC-BUILD2), Mosayk (D. Malomo, R. Pinho), 31st October 2017.
6. Experimental campaign on a clay URM full-scale specimen representative of the Groningen building stock (EUC-BUILD2), Eucentre (F. Graziotti, U. Tomassetti, A. Rossi, B. Marchesi, S. Kallioras, M. Mandirola, A. Fragomeli, E. Mellia, S. Peloso, F. Cuppari, G. Guerrini, A. Penna, G. Magenes, G), 20th July 2016.
7. EUC-BUILD2: Modelling predictions and analysis cross-validation of detached single-storey URM Building, ARUP, TU Delft, Eucentre and Arcadis (several staff members from all four institutions), 30th September 2016



NAM

Title	Using the Applied Element Method to model the shake-table testing of two full-scale URM houses		Date	October 2017
			Initiator	NAM
Autor(s)	Daniele Malomo and Rui Pinho	Editors	Jan van Elk and Dirk Doornhof	
Organisation	Modelling and Structural Analysis Konsulting (Mosayk)	Organisation	NAM	
Place in the Study and Data Acquisition Plan	<p><u>Study Theme:</u> Seismic Response of Buildings (URM)</p> <p><u>Comment:</u> Many of the buildings in the Groningen field area are terraced unreinforced masonry buildings. A program to assess the response of these building to earthquakes was therefore initiated. This program built on the experimental and modelling program into the properties of URM building materials, wall elements and wall units. A typical Groningen terraced house built using materials from the Groningen area by builders from the Groningen area, was tested at the shake-table of Eucentre in Pavia, Italy (Ref. 1). Although the building was at the end of this test program seriously damaged, the building had not collapsed. This left questions on the remaining capacity of the structure and its ability to resist larger seismic movements before (partially) collapsing. The test in Eucentre was therefore followed-up with further tests at the laboratory of LNEC in Lisbon, Portugal (Ref. 2 to 5). Here the upper floors of the building tested in Eucentre were re-built in the LNEC laboratory and subjected to movements measured at the base of the upper floors in Eucentre. Additionally, detached terraced unreinforced masonry building was built in the Eucentre laboratory and was tested at the shake-table (Ref. 6 and 7). Also this building was constructed using materials from the Groningen area by builders from the Groningen area. This report shows the results of modelling of these two shake-table testing programs obtained by Mosayk using Extreme Loading for Structures (ELS), a commercial structural analysis software based on the Applied Element Method (AEM) after such tests, describing also the calibration process of the AEM numerical model.</p>			
Directly linked research	(1) Shake table tests (2) Fragility curves for building typologies (URM) (3) Risk Assessment			
Used data	Experiments			
Associated organisation	NAM			
Assurance	Modelling and Structural Analysis Konsulting (Mosayk)			

D5

DELIVERABLE

Project Information

Project Title: **Advanced modelling of URM buildings in support of fragility/consequence functions derivation**

Project Start: May 2016

Duration: 20 months

Technical Point of Contact: Rui Pinho

Administrative Point of Contact: Roberto Nascimbene

Deliverable Information

Deliverable Title: **Using the Applied Element Method to model the shake-table testing of two full- scale URM houses**

Data of Issue: 31st October 2017

Author: Daniele Malomo

Reviewer: Rui Pinho

REVISION: **v1**

Table of Contents

Executive Summary	4
Nomenclature	5
1 Introduction	6
1.1 Scope	6
1.2 Analysis method.....	6
2 EUC-BUILD1	6
2.1 Building prototype.....	6
2.2 Mechanical properties of masonry	7
2.3 Testing procedure	7
2.4 Brief overview of test specimen response.....	8
2.5 Numerical model.....	9
2.6 Post-test material properties	10
2.7 Summary of results.....	11
2.8 Floor hysteresis.....	13
2.9 Roof acceleration hysteresis.....	14
2.10 Global hysteresis.....	16
2.11 Crack patterns and collapse mechanism	17
3 EUC-BUILD2	20
3.1 Building prototype.....	20
3.2 Mechanical properties of masonry	20
3.3 Testing procedure	21
3.4 Brief overview of test specimen response.....	21
3.5 Numerical model.....	22
3.6 Post-test material properties	23
3.7 Summary of results.....	23
3.8 Floor hysteresis.....	25
3.9 Roof acceleration hysteresis.....	27
3.10 Global hysteresis.....	28
3.11 Crack patterns and collapse mechanism	30
4 Closing Remarks	33
References	34
Appendix A – further details on URM model building in ELS.....	35
A.1 AEM modelling of contact surfaces between elements.....	35

<i>A.1.1 Nailed connections between beam and plank elements</i>	36
<i>A.1.2 Definition of “weak” and “cracked” mortar spring interfaces</i>	38
A.2 Numerical modelling of plank elements.....	39
A.3 Connectors, ties and steel anchors elements	41
A.4 Derivation of mortar Young’s modulus from homogenisation formulae.....	42
A.5 References	44

Executive Summary

Within the framework of the research programme on hazard and risk of induced seismicity in the Groningen region, sponsored by the Nederlandse Aardolie Maatschappij BV (NAM), both a two-storey URM cavity wall (EUC-BUILD1) and a one-storey double-leaf (EUC-BUILD2) full-scale URM house specimens were tested in 2015 at the shake-table of the European Centre of Training and Research in Earthquake Engineering (Eucentre - Pavia, Italy).

This report shows the results obtained by Mosayk using Extreme Loading for Structures (ELS), a commercial structural analysis software based on the Applied Element Method (AEM) after such tests, describing also the calibration process of the AEM numerical model.

Even if some further improvements are needed for both models (e.g. the roof response of EUC-BUILD2 was not well captured during the first runs), they are able to reproduce adequately the overall structural behaviour exhibited by the specimens during the testing phases in terms of capacity, deformation and crack patterns.

Nomenclature

Symbol	Description
ρ	Mass density [kg/m^3]
E	Masonry Young's modulus [MPa]
E_{mo}	Mortar Young's modulus [MPa]
E_{u}	Unit Young's modulus [MPa]
ν	Poisson's ratio of masonry
f_{m}	Masonry compressive strength [MPa]
f_{w}	Flexural bond strength of mortar joints [MPa]
f_{v0}	Masonry (bed joint) initial shear strength (cohesion) [MPa]
μ	Masonry (bed joint) shear friction coefficient

1 Introduction

1.1 Scope

The test specimen EUC-BUILD1 built in the Eucentre laboratory in Pavia is a full-scale cavity wall two-storey building. The loadbearing masonry was composed of calcium silicate bricks, sustaining two reinforced concrete floors, whereas two gable walls supported a pitched timber roof (Graziotti et al., 2015a).

The single-storey full-scale test-building EUC-BUILD2 (built and tested at the Eucentre laboratory in Pavia as well) is instead a prototype structure representative of a detached house, common in the region of Groningen. Indeed, it was designed to combine several common features of detached houses pre 1940's such as the double-wythe URM walls characterised by a Dutch Cross bond brickwork and the wooden roof structure (Kallioras et al., 2017).

These experimental studies were aimed at enhancing further the knowledge of the dynamic response of this type of structures by dynamically testing them all the way up to near-collapse conditions. For this purpose, drift limits for different performance levels, damage evolution for increasing shaking levels, storey accelerations amplified along the building height, and displacement/drift profiles for increasing shaking intensity were constantly monitored during the tests and scrutinised. In particular, specific attention was paid to the dynamic performance of the roof structure and on the possible activation of gable out-of-plane mechanisms.

With a view to validate the use of the Applied Element Method (Meguro and Tagel-Din, 2000, 2001, 2002) in modelling these URM building typologies, Mosayk modelled both test specimens using ELS - Extreme Loading for Structures (ASI, 2017), an AEM-based commercial structural analysis software. This report thus describes such modelling efforts by Mosayk.

1.2 Analysis method

According to the Applied Element Method (AEM), a given structure is discretised as a virtual assembly of small rigid units, carrying only mass and damping of the system, connected by linear and nonlinear springs (with normal stiffness k_n and shear stiffness k_s) in which the material properties are lumped. It is noted that, even if the single mesh element is rigid, the behaviour of the whole assembly is deformable. Thus, a masonry wall segment can be represented by means of units (fully rigid or deformable) linked by dimensionless mortar layers (simplified micro-modelling). The theoretical formulation allows reproducing the structural response both in the finite and discrete numerical domains, taking into account contacts and dynamic element interactions automatically. In addition to the pioneering publications listed above, further details on the AEM formulation may be found in e.g. Mosayk (2016) and Malomo (2018).

2 EUC-BUILD1

2.1 Building prototype

The test-house was a full-scale two-storey building, with a timber roof and RC slabs, 5.82 m long, 5.46 m wide and 7.76 m high with a total mass of 56.4 t. The walls, supported by a steel-concrete composite foundation, consisted of two unreinforced masonry leaves. The inner loadbearing leaf was made of calcium silicate (CS) bricks whereas the external leaf was a clay brick (CL) veneer without any loadbearing function. The inner CS masonry was continuous along the entire perimeter of the house, while the outer clay brick leaf was not present in the South façade.

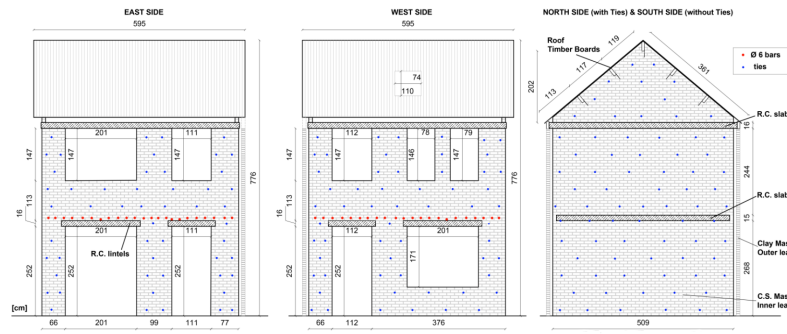


Figure 1 Elevation views of the specimen's CS inner leaf (Graziotti et al., 2015b)

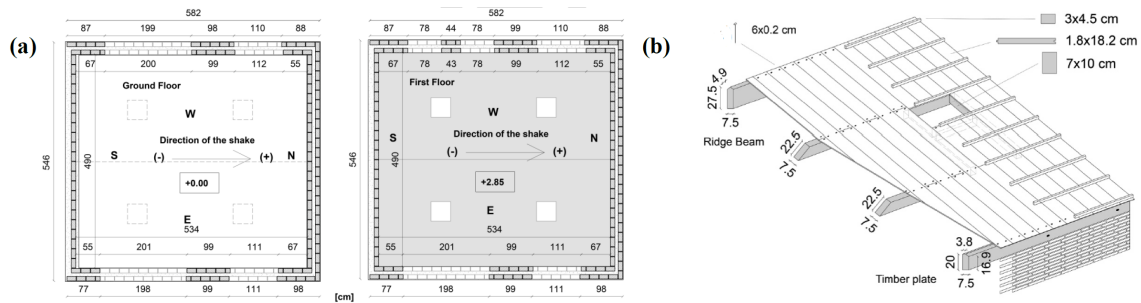


Figure 2 Plan view of the ground floor (left) and details of roof structure (right) (Graziotti et al., 2015b)

2.2 Mechanical properties of masonry

Both CS and CL masonry components were tested at Eucentre in order to characterise the masonry material and obtain the mechanical properties reported in Table 1, below. Such properties are referred to the final components test values reported in Graziotti et al. (2015b).

Table 1 Preliminary and post-test material properties

Symbol	CS	CL
ρ	1835	1905
E	4182 ¹	6033 ¹
E_{mo}	---	---
E_u	---	---
ν	---	---
f_m	6.20	11.32
f_w	0.0056	0.152
f_{v0}	0.035	0.15
μ	0.42	0.70

¹ Secant stiffness to 10% f_m

2.3 Testing procedure

The building specimen constructed on the shake-table of Eucentre was subjected to incremental dynamic tests, i.e. a series of shake-table runs under input motions of increasing intensity up to near-collapse of the structure. Two different ground motions had been selected for the EUC-BUILD1 test, EQ1 and EQ2 (Graziotti et al., 2015). In Figure 3 below the considered acceleration time-histories are reported. The sequence of the input motions, the relative scaled factors applied and the associated horizontal peak ground accelerations (PGA) are summarised in Table 2.

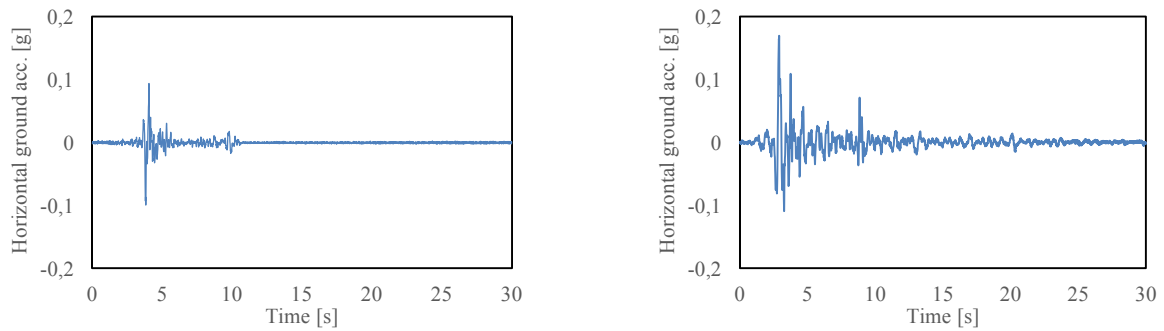


Figure 3 EQ1@100 (left) and EQ2@100 (right) horizontal seismic inputs

Table 2 EUC-BUILD1 test sequence

Test ID	Test Input	Test Name	Nominal PGA [g]	Recorded PGA [g]
1	EQ1	EQ1@25%	0.024	0.024
2	EQ1	EQ1@50%	0.049	0.050
3	EQ1	EQ1@100%	0.096	0.099
4	EQ1	EQ1@150%	0.144	0.137
5	EQ2	EQ2@100%	0.159	0.170
6	EQ2	EQ2@125%	0.199	0.194
7	EQ2	EQ2@150%	0.239	0.243
8	EQ2	EQ2@200%	0.319	0.307

2.4 Brief overview of test specimen response

In this section, the structural behaviour exhibited by the specimen is briefly recalled, according to the description reported in Graziotti et al. (2015a). The building sustained shaking of $PGA = 0.14g$ (EQ1@150%) with no visible damage and was in a near-collapse state after testing at EQ2@200%, when the test sequence was stopped. The most relevant cracks are reported in Figure 4.

The first significant cracks observed in the CS masonry of the second storey were recorded after the test EQ2@150%. A horizontal crack developed along the base of the squat pier of the second storey, on the West side, indicative of the pier's bending-rocking response. This crack was further extended with a stair-stepped diagonal pattern to the centre of the adjacent spandrel. Until this intensity level no damage in the two transverse walls was detected.

The building experienced a substantial level of damage (compared to that observed under lower intensity shaking) after the test EQ2@200%. As far as the damage reported in the transversal walls is concerned, the formation of 45° stair-stepped diagonal cracks was clearly observed. This could be associated with the activation of an out-of-plane two-way bending mechanism. Focusing on the gables, horizontal cracks along their base were indicative of an out-of-plane overturning mechanism activated at the gable level. Regarding the damage noticed in the veneer walls, perceptible cracks developed only during the last test, EQ2@200%.

More details about the experimental procedure and the specimen response can naturally be found in the dedicated test report (Graziotti et al. 2015b). In what follows, the most relevant experimental results are shown and compared to the numerical results obtained with the analyses carried out after the test.

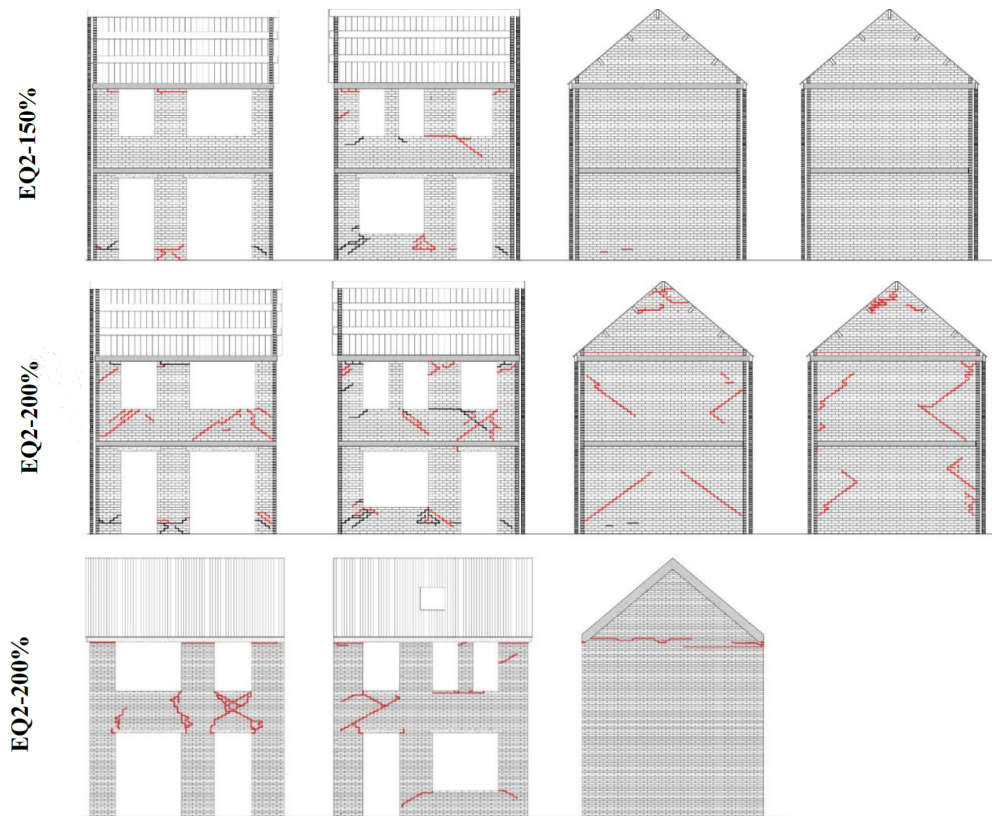


Figure 4 Significant damage detected at EQ2@150 and EQ2@200 to the East, West, North and South CS inner walls and cracks detected during EQ2@200 to the CL walls (Graziotti et al. 2015b).

2.5 Numerical model

The most relevant modelling assumptions related to the numerical model (Figure 5) built after the test are briefly summarised in Table 3 below, and further discussed, justified and detailed in Appendix A.

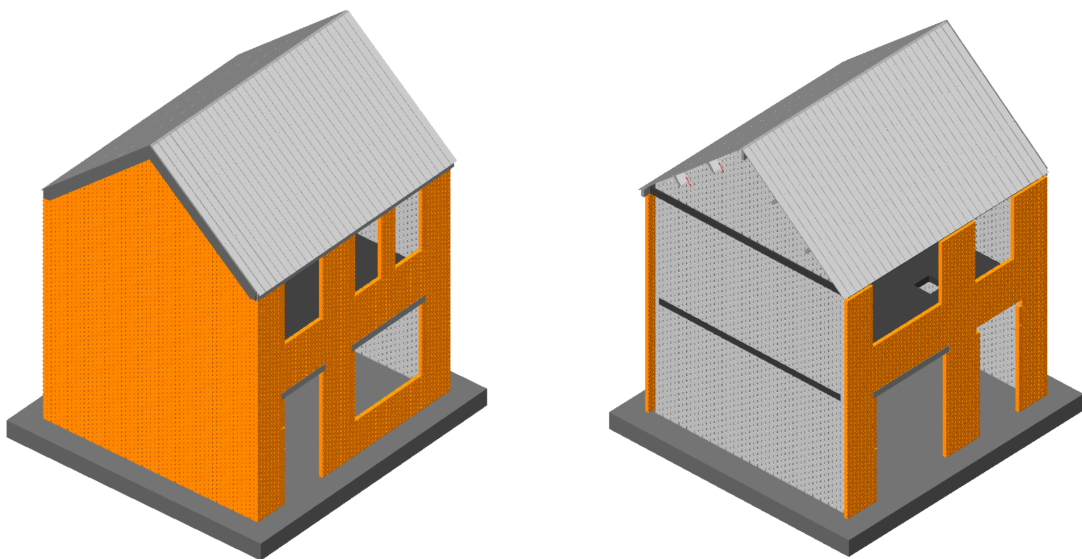


Figure 5 Screenshots of the EUC-BUILD1 numerical model

Table 3 EUC-BUILD1 modelling assumptions

Input	Modelling assumption
Boundary condition	Structure connected by mortar interfaces to a fixed slab
Roof diaphragm	Nailed connection between planks and beams modelled as equivalent spring interfaces characterised by an elastic-perfectly-plastic behaviour
Wall ties	Elastic-perfectly-plastic beam elements
First floor slab-front/back inner leaves connection	Mortar interface
Second floor slab-front/back inner leaves connection	Weak mortar interface (since the gap between the slab and the wall was filled after the temporary supports removal, i.e. after RC slab deflection)
Timber beam-front/back outer leaves connection	Weak mortar interface (since the gap between the slab and the wall was filled after the temporary supports removal, i.e. after RC slab deflection)
First and second floor slab and end/party walls connection	Mortar interface
Connection between roof girders and end/party walls	Mortar interface plus elastic-perfectly plastic L-steel anchors
Wall-to-wall connection	45-degrees connections between adjacent walls (see Figure 6)

The material properties of both CS and CL masonry were updated in light of the data provided by the characterisation tests, as reported in Graziotti et al. (2015b). The geometrical connections between wall elements were further investigated in order to evaluate their influence on both in-plane and out-of-plane structural response, and a 45-degrees wall-to-wall interface joint (see Figure 6c) was then adopted for both CS and CL walls. Different values of tensile strength (i.e. direct and flexural bond strength) were used in the model for longitudinal and transverse walls, as well as for the wall-to-wall connections, which were based on the expected structural behaviour.

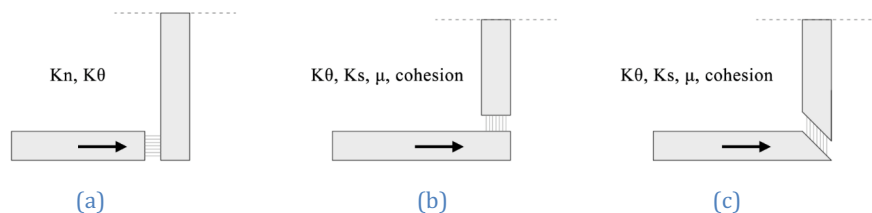


Figure 6 (a) (b) (c) Different types of wall-to-wall connections that may be employed with the AEM

2.6 Post-test material properties

In Table 4 and Table 5 below, the final material characterisation test values, as well as values assumed for the modelling of both the CS and CL masonry, are reported.

Table 4 CS masonry characterisation test and numerical properties

Symbol	Description	Test value ⁴	Employed value
ρ	Mass density [kg/m^3]	1835	1835
E	Masonry Young's modulus [MPa]	4182 ¹	---
E_{mo}	Mortar Young's modulus [MPa]	---	4700 ²
E_u	Unit Young's modulus [MPa]	---	2577 ²
ν	Poisson's ratio of masonry	---	0.25
f_m	Masonry compressive strength [MPa]	6.20	---
f_{mo}	Mortar compressive strength [MPa]	5.79	18.67
f_u	Brick compressive strength [MPa]	45.81	45.81
f_w	Flexural bond strength of mortar joints [MPa]	0.056	0.056
f_t	Tensile strength of mortar joints [MPa]	---	0.91 ³
f_{v0}	Masonry (bed joint) initial shear strength (cohesion) [MPa]	0.035	0.21
μ	Masonry (bed joint) shear friction coefficient	0.42	0.42

Table 5 CL masonry characterisation test and numerical properties

Symbol	Description	Test value ⁴	Employed value
ρ	Mass density [kg/m^3]	1905	1905
E	Masonry Young's modulus [MPa]	6033 ¹	---
E_{mo}	Mortar Young's modulus [MPa]	---	6033 ⁴
E_u	Unit Young's modulus [MPa]	---	12169 ²
ν	Poisson's ratio of masonry	---	0.25
f_m	Masonry compressive strength [MPa]	6.20	---
f_{mo}	Mortar compressive strength [MPa]	7.40	18.67
f_u	Brick compressive strength [MPa]	18.67	18.67
f_w	Flexural bond strength of mortar joints [MPa]	0.15	0.15
f_t	Tensile strength of mortar joints [MPa]	---	0.81 ⁴
f_{v0}	Masonry (bed joint) initial shear strength (cohesion) [MPa]	0.035	0.035
μ	Masonry (bed joint) shear friction coefficient	0.70	0.70

¹ Secant stiffness to 10% f_m

² Inferred by means of empirical formulae (Ciesielski 1999; ICBO 1991; Matysek and Janowski 1996; Brooks and Baker 1998)

³ Inferred by means of empirical formulae (Kim and Reda Taha, 2014)

⁴ E_{mo} was in this case taken as equal to E, since inferring it through the customary formulae was leading to abnormally high values, as a consequence of the equally unexpectedly large experimental clay brick Young's module (E_u) value

2.7 Summary of results

The numerical outcomes obtained are summarised below, in the form of hysteresis envelope plots and deflected shape prior to collapse.

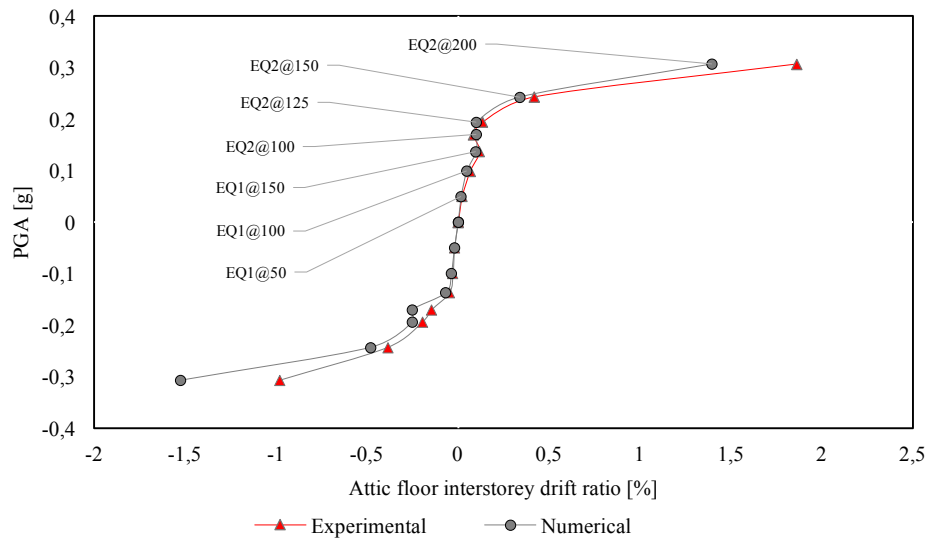


Figure 7 IDA: PGA vs attic floor IDR¹

¹ PGA vs. attic floor interstorey drift ratio (IDR) IDA curve plots the PGA [g] vs. the positive and negative direction IDR envelopes of attic floor [%] for each test.

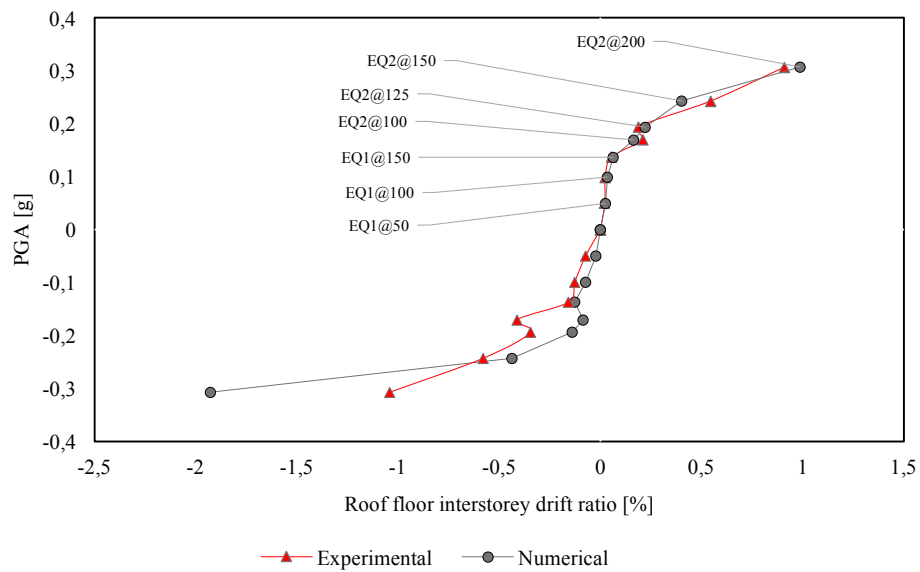


Figure 8 IDA: PGA vs roof floor IDR¹

¹ PGA vs. roof interstorey drift ratio (IDR) IDA curve plots the PGA [g] vs. the positive and negative direction IDR envelopes of roof [%] for each test.

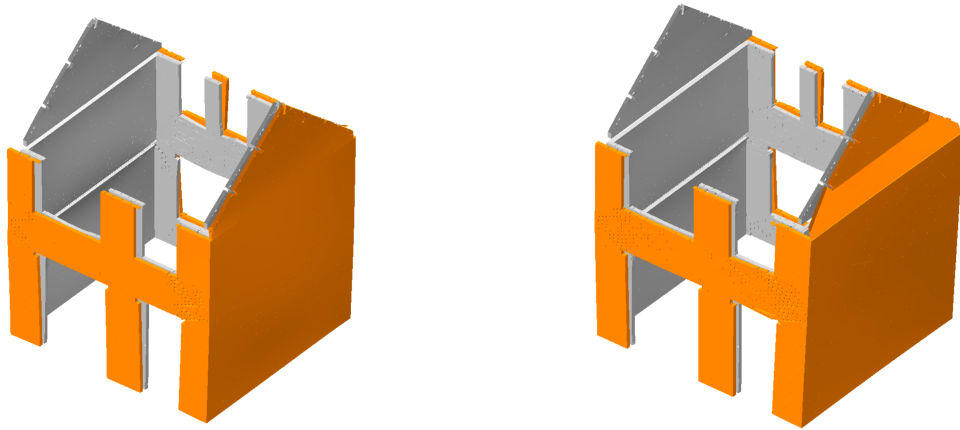


Figure 9 Deflected shapes (magnified x10) at maximum excursion prior to the end of test at EQ2@100 (left) and EQ2@150 (right)

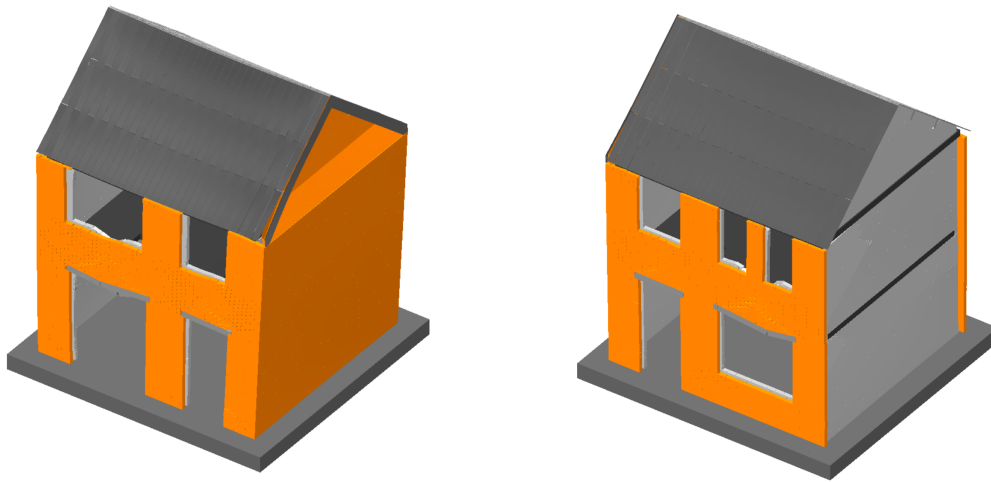
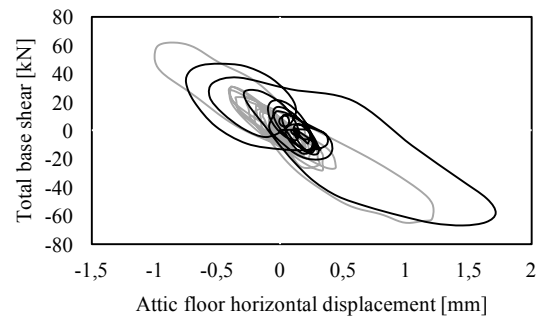
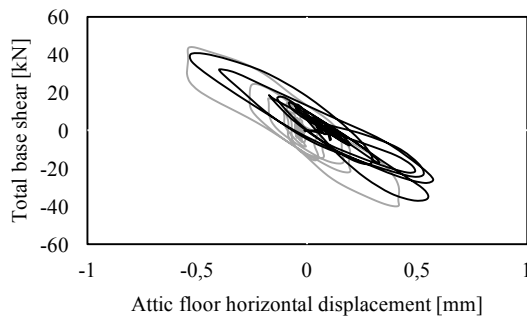
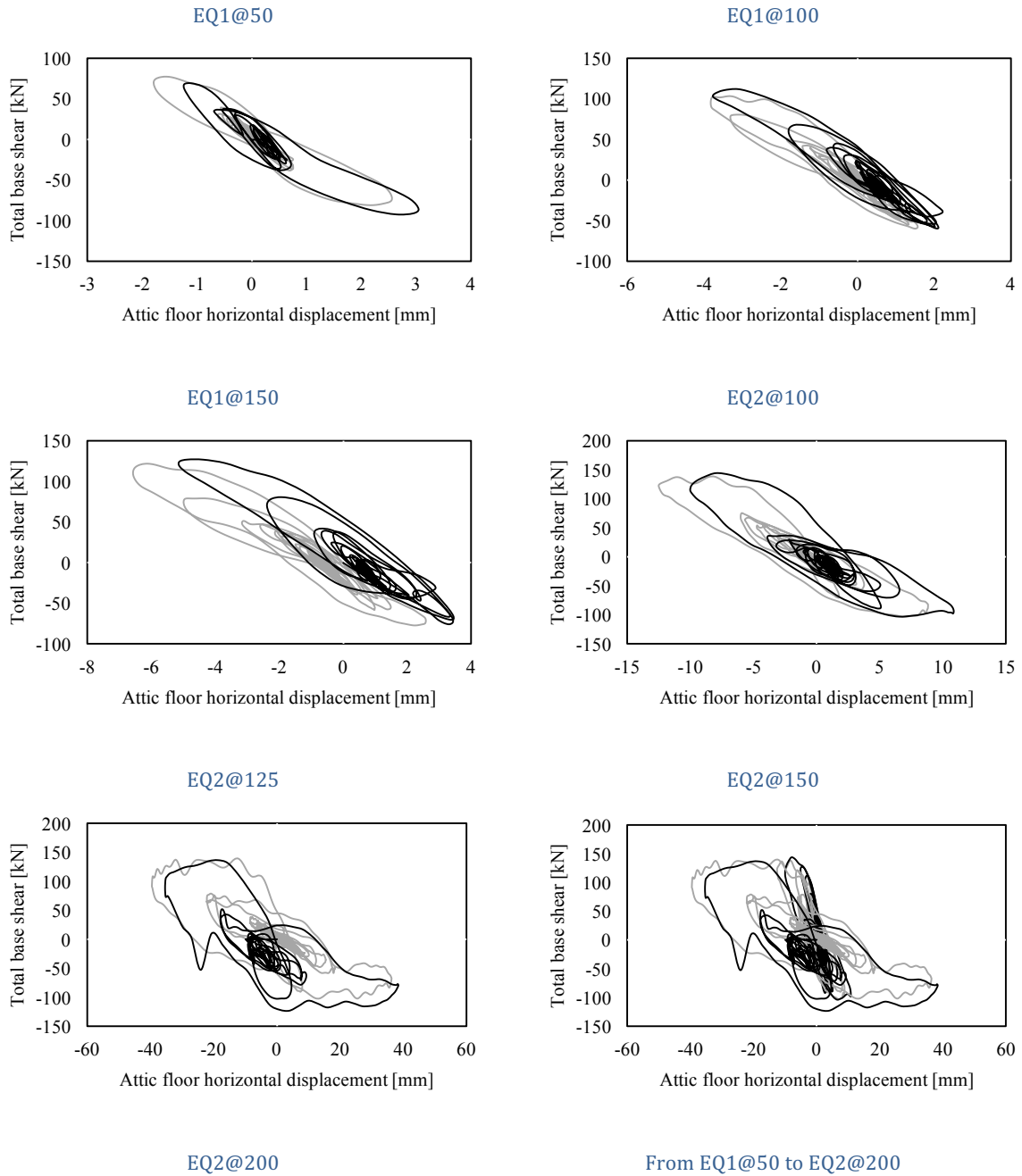


Figure 10 Gable out-of-plane mechanism, slender piers rocking and damage of the spandrels (magnified x5)

2.8 Floor hysteresis

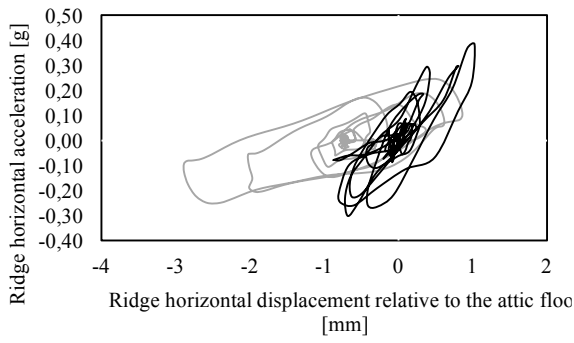
Floor hysteresis is defined as the total “base” shear [kN] vs. attic floor horizontal displacement relative to the base [mm]. Grey is experimental and black is numerical.



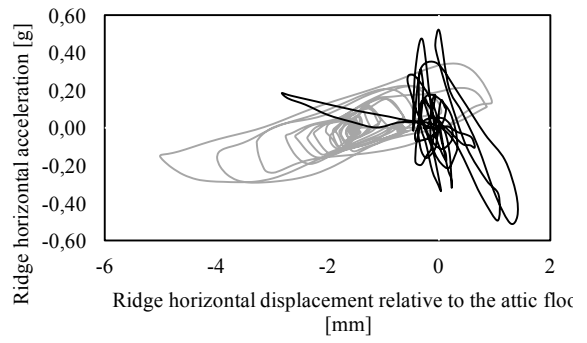


2.9 Roof acceleration hysteresis

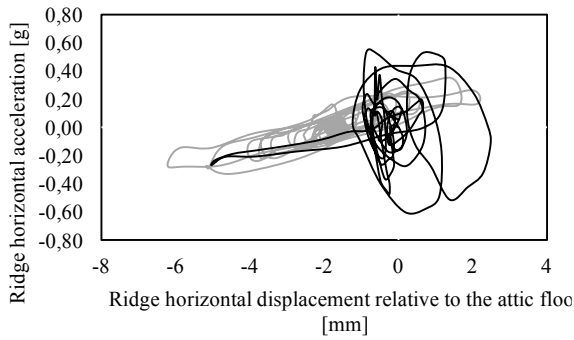
Roof acceleration hysteresis is defined as the ridge horizontal acceleration [g] vs. ridge horizontal displacement relative to the attic floor horizontal displacement [mm]. Grey is experimental and black is numerical.



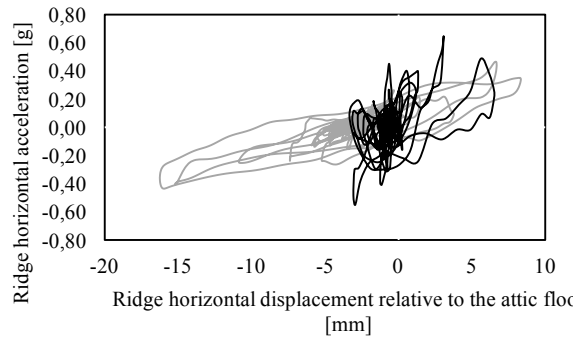
EQ1@50



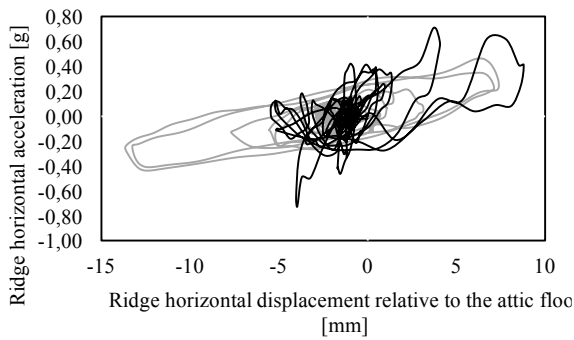
EQ1@100



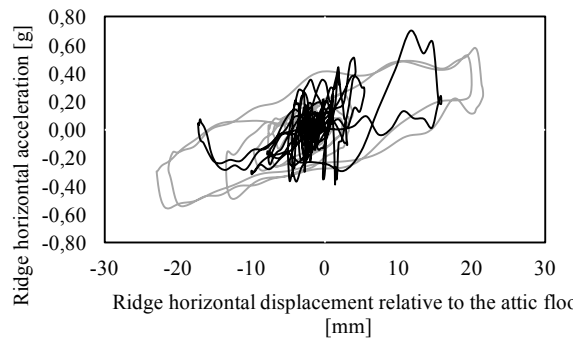
EQ1@150



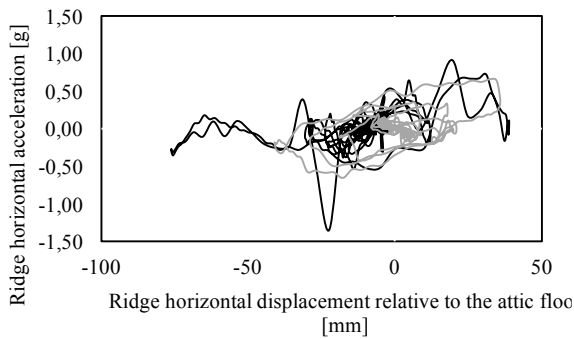
EQ2@100



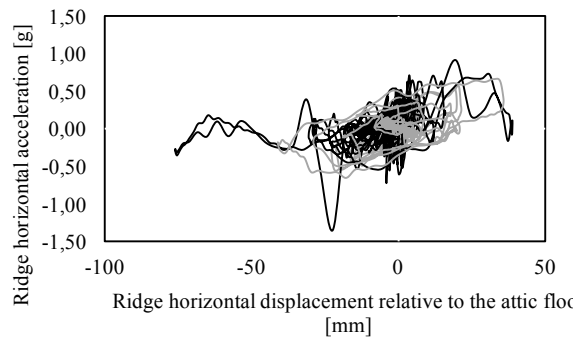
EQ2@125



EQ2@150



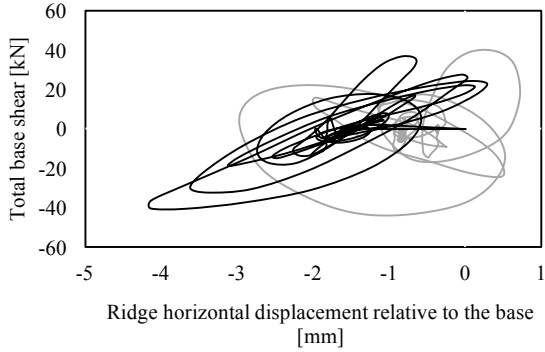
EQ2@200



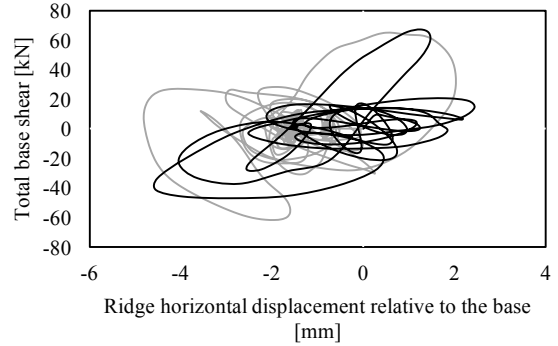
From EQ1@50 to EQ2@200

2.10 Global hysteresis

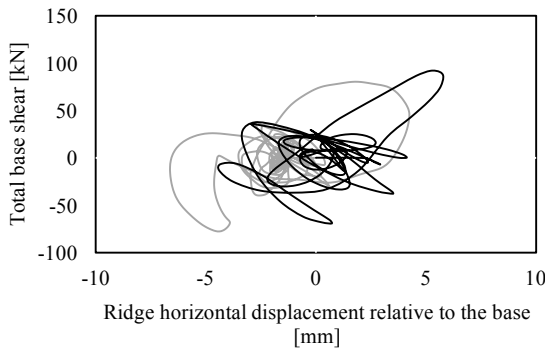
Global hysteresis is the total “base” shear [kN] vs. ridge hor. displacement relative to the base [mm]. Grey is experimental and black is numerical.



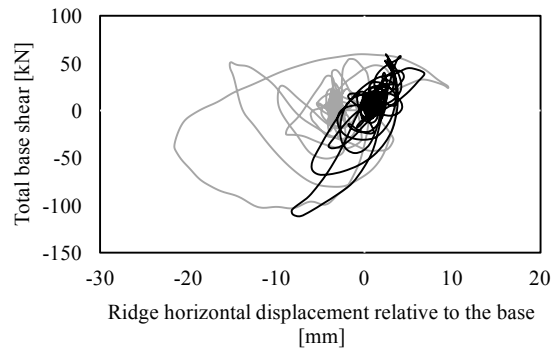
EQ1@50



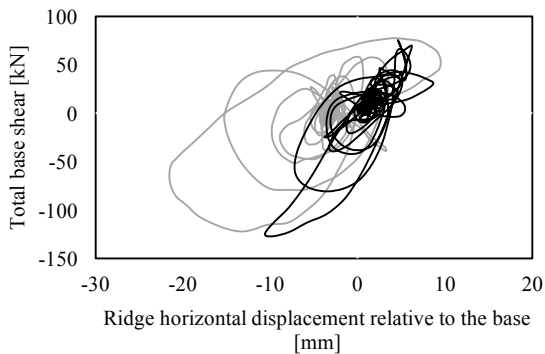
EQ1@100



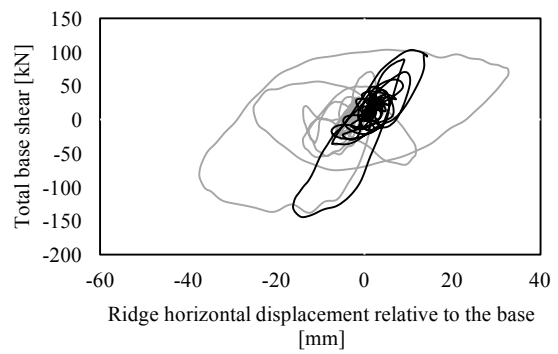
EQ1@150



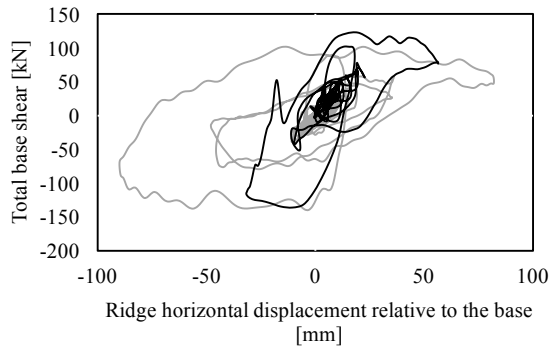
EQ2@100



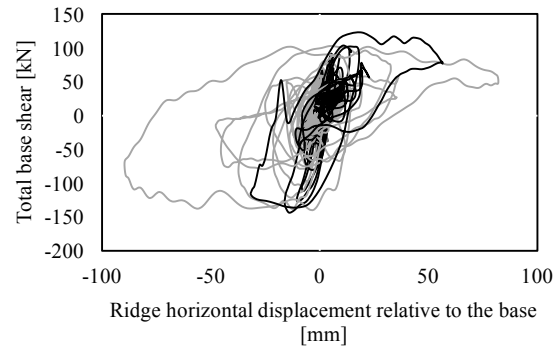
EQ2@125



EQ2@150



EQ2@200



From EQ1@50 to EQ2@200

2.11 Crack patterns and collapse mechanism

The final damage predictions for each wall (both CS and CL masonry elements) are compared in this sub-section with their experimental counterpart (varied magnification).

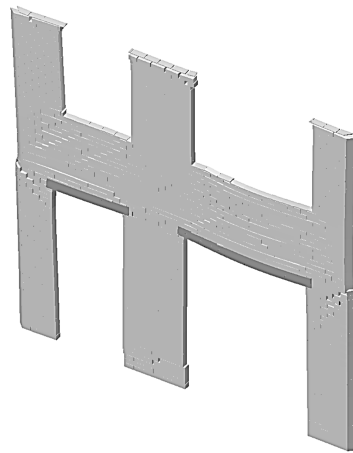
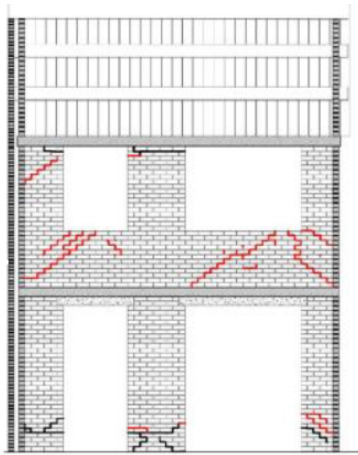


Figure 11 EQ2@200 _ Experimental (left) and numerical (right) damage plot of inner leaf – front wall

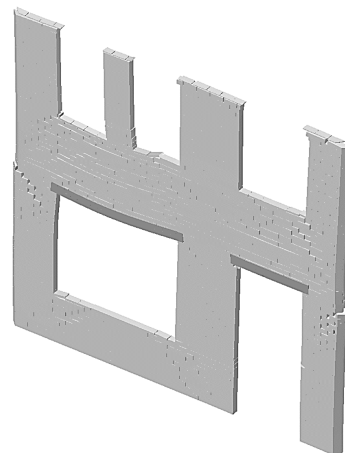
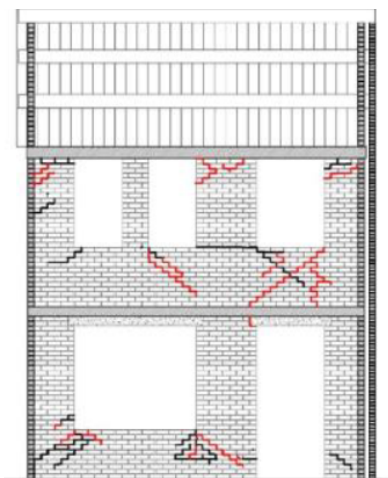


Figure 12 EQ2@200 _ Experimental (left) and numerical (right) damage plot of inner leaf – back wall

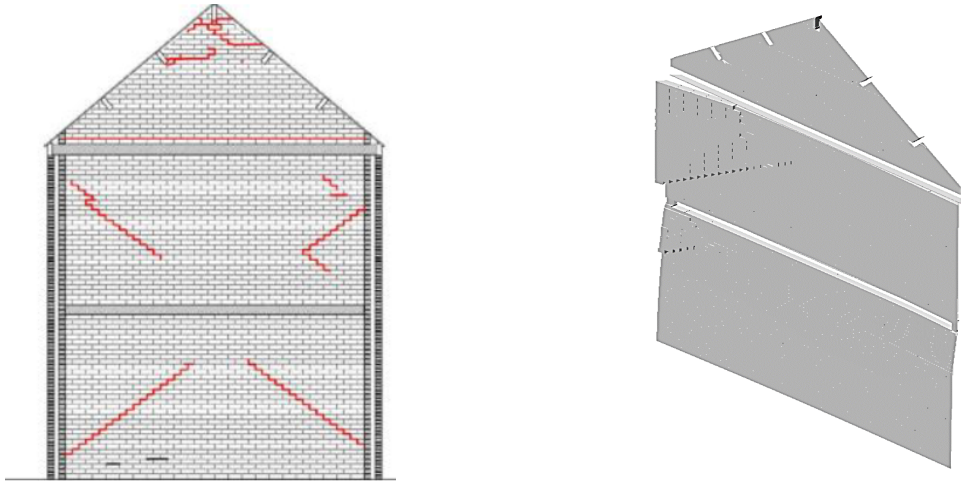


Figure 13 EQ2@200 _ Experimental (left) and numerical (right) damage plot of inner leaf – end wall

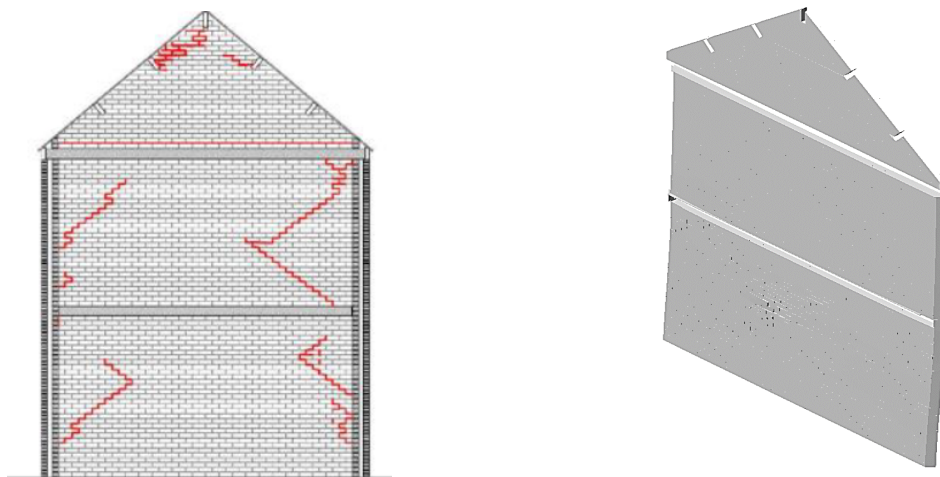


Figure 14 EQ2@200 _ Experimental (left) and numerical (right) damage plot of inner leaf – party wall

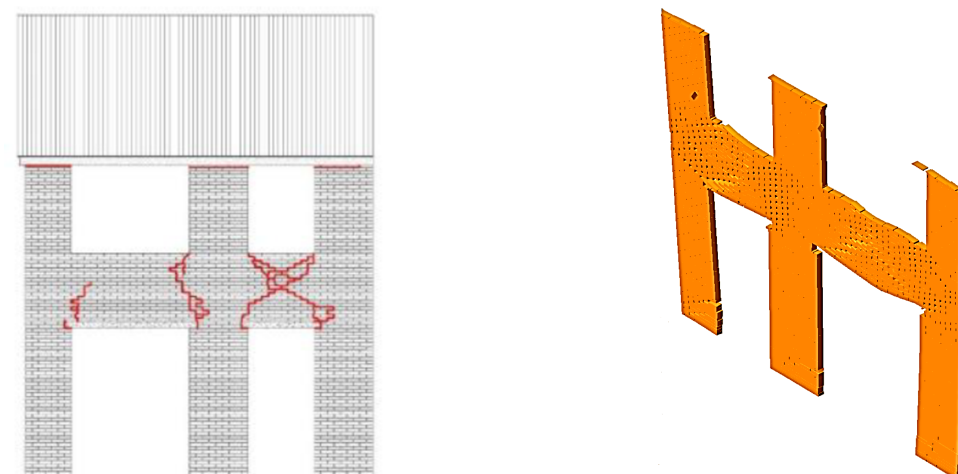


Figure 15 EQ2@200 _ Experimental (left) and numerical (right) damage plot of outer leaf – front wall

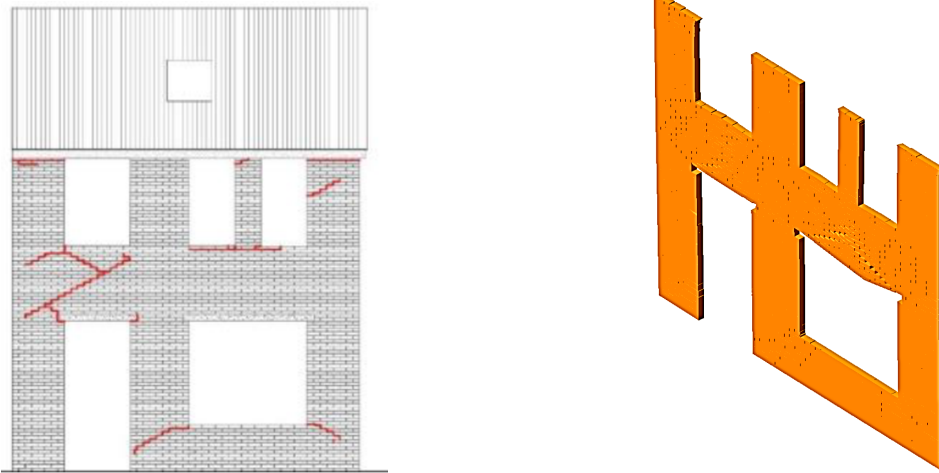


Figure 16 EQ2@200 _ Experimental (left) and numerical (right) damage plot of outer leaf – back wall

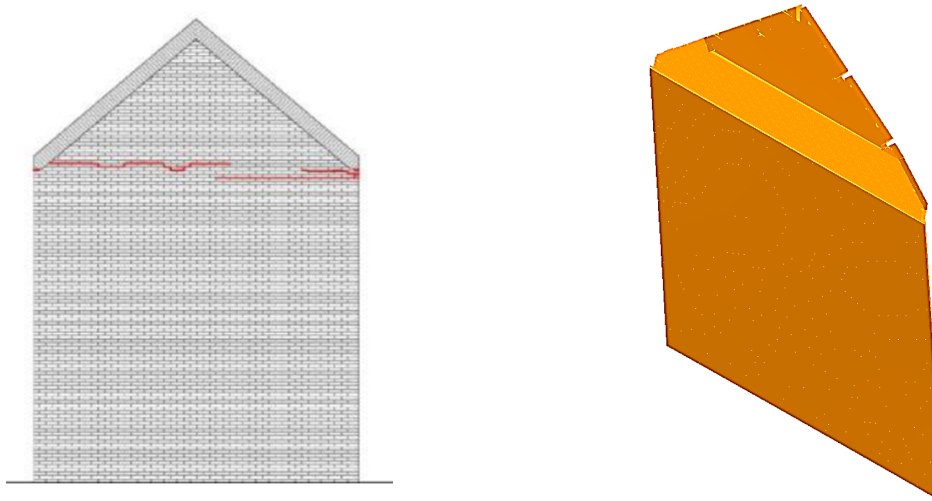


Figure 17 EQ2@200 _ Experimental (left) and numerical (right) damage plot of outer leaf – end wall

3 EUC-BUILD2

3.1 Building prototype

The in-plan dimensions of the specimen were 5.33 m x 5.77 m, with a height of about 6.23 m. The total mass was 32.6 t. As mentioned above, the loadbearing structural system is provided by 208-mm-thick, double-wythe unreinforced masonry walls. The brickwork bond adopted is called Dutch Cross bond, as reported in Figure 19.

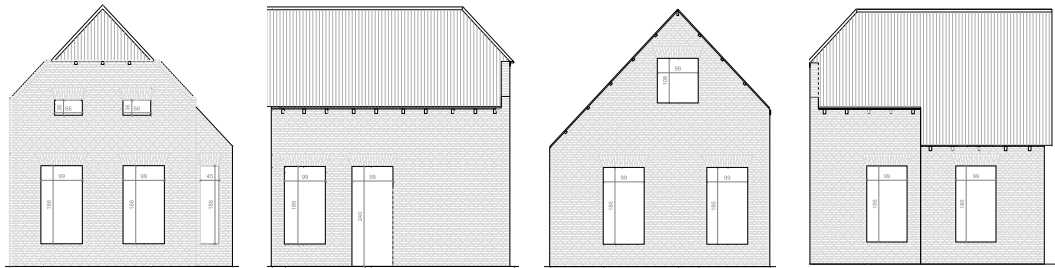


Figure 18 Elevation views of the specimen (Kallioras et al. 2017)

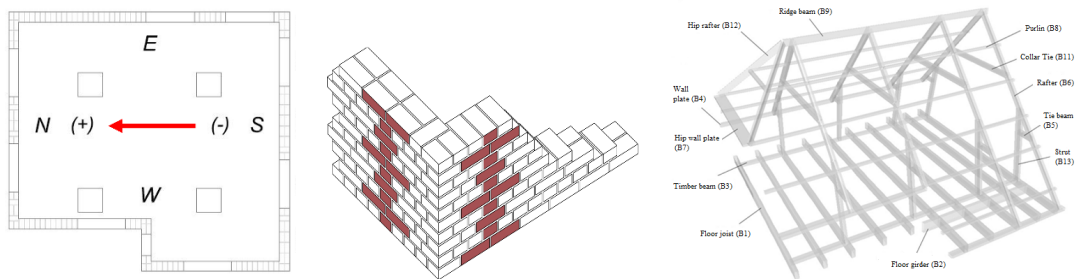


Figure 19 Plan view of the ground floor (left), Dutch cross bond representation and details of roof structure (right) (Graziotti et al., 2016)

3.2 Mechanical properties of masonry

CL masonry components were tested at Eucentre in order to characterise the masonry material and obtain the mechanical properties reported in Table 6, below. Such properties are referred to the final components test values reported in Graziotti et al. (2016)

Table 6 EUC-BUILD2 material properties

Symbol	CL
ρ	2101
E	6519 ¹
E_{mo}	---
E_u	---
ν	---
f_m	9.23
f_w	0.23
f_{v0}	0.26
μ	0.55

¹ Secant stiffness to 10% f_m

3.3 Testing procedure

The specimen was subjected to incremental dynamic tests, applying a series of shake-table motions of increasing intensity to assess damage evolution, failure modes, and ultimate capacity of the building. The same ground motions previously introduced for EUC-BUILD1 were applied (see Figure 20): a first record, labelled EQ1, with peak ground acceleration PGA = 0.096 g; and a second record, termed EQ2, had PGA = 0.159 g. Additional scaled inputs were considered according to the loading sequence reported in Table 7.

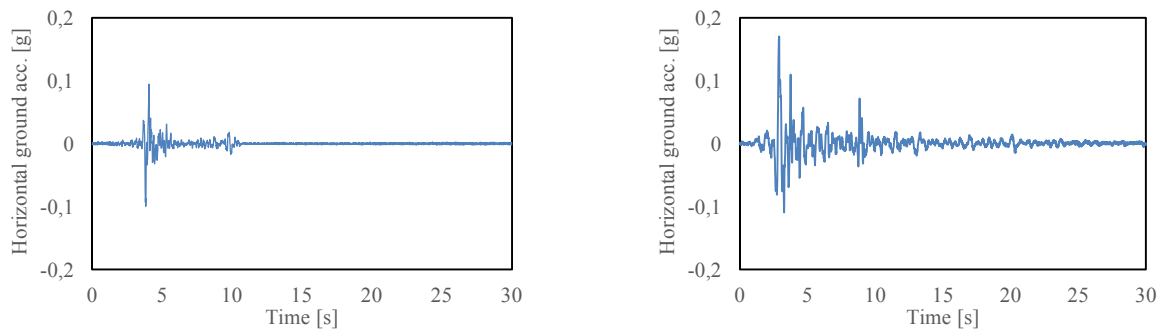


Figure 20 EQ1@100 (left) and EQ2@100 (right) horizontal seismic inputs

Table 7 EUC-BUILD2 test sequence

Test ID	Test Input	Test Name	Nominal PGA [g]	Recorded PGA [g]
1	EQ1	EQ1@25%	0.024	0.024
2	EQ1	EQ1@50%	0.049	0.050
3	EQ1	EQ1@100%	0.096	0.099
4	EQ1	EQ1@150%	0.144	0.137
5	EQ2	EQ2@50%	0.077	0.080
6	EQ2	EQ2@100%	0.159	0.140
7	EQ2	EQ2@150%	0.232	0.227
8	EQ2	EQ2@200%	0.319	0.293
9	EQ2	EQ2@250%	0.387	0.392
10	EQ2	EQ2@300%	0.500	0.346
11	EQ2	EQ2@400%	0.620	0.679

3.4 Brief overview of test specimen response

The tested building behaviour was mainly governed by the out-of-plane response of the gables, albeit diffuse damage was also observed with activation of both in-plane and out-of-plane failure mechanisms involving all of the façades of the building. The specimen exhibited relevant damage only at EQ2@150, consisting of horizontal hairline cracks forming on the South façade, a few centimetres above the floor level. During shaking under EQ2@300 a global response of the structure was triggered, as evidenced by the formation of new cracks and the propagation of pre-existing ones. Out-of-plane mechanisms developed on both gables. After the EQ2@400% test widespread damage was observed throughout the building, which was deemed to have reached near-collapse conditions. The final crack pattern of Figure 21 shows the contribution of portions of the North and South façades as flanges for the in-plane response of the longitudinal corner piers.



Figure 21 Significant damage detected at EQ2@300 and EQ2@400, (Graziotti et al. 2016)

More details about the experimental procedure and the specimen response can naturally be found in the dedicated test report (Graziotti et al., 2016). In what follows, the most relevant experimental results are shown and compared to the numerical results obtained with the analyses carried out after the test.

3.5 Numerical model

The most relevant modelling assumptions related to the numerical model built after the test (Figure 22) are briefly summarised in Table 8 below, and further discussed, justified and detailed in Appendix A.

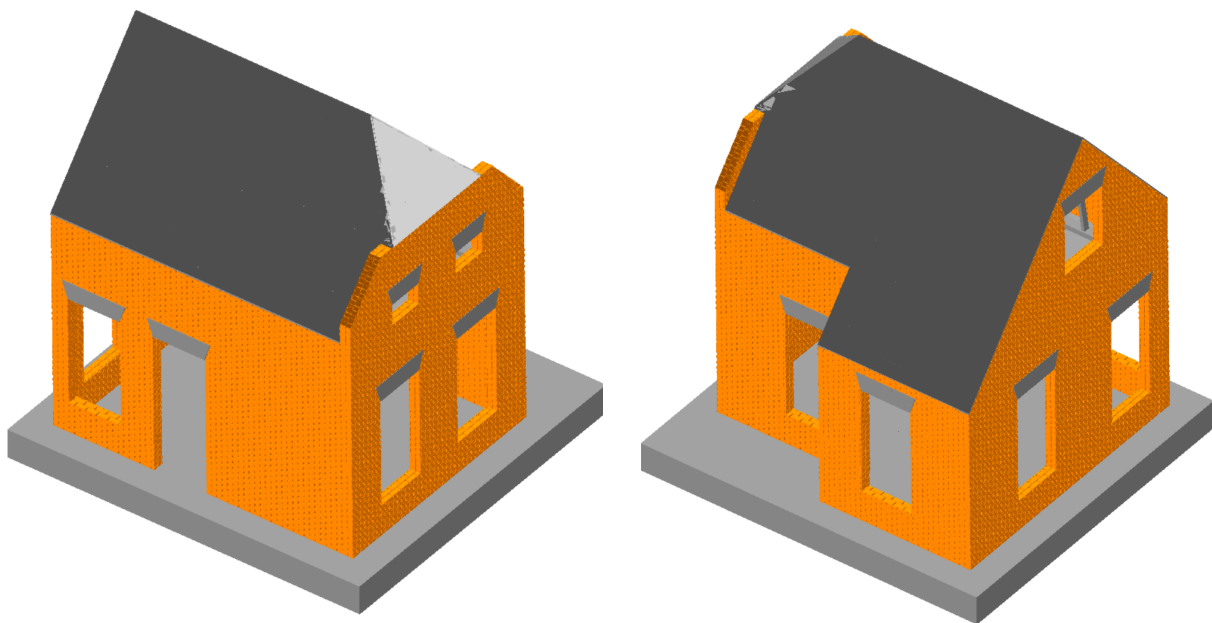


Figure 22 Screenshots of the EUC-BUILD2 numerical model

Table 8 EUC-BUILD2 modelling assumptions

Input	Modelling assumption
Boundary condition	Structure connected by mortar interfaces to a fixed slab
Roof diaphragm	Equivalent membrane elements
First-floor diaphragm/wall connection	Mortar interface
Timber beam/wall connection	Mortar interface
Connection between roof girders and wooden diaphragm	Nailed connection between membrane and beams modelled as equivalent spring interfaces characterised by an elastic-perfectly-plastic behaviour
Wall-to-wall connection	45-degrees connections between adjacent walls (see Figure 6)
Double-leaf brickwork	The influence of brick arrangement was not accounted (i.e. no perpendicular bricks to the bed joints were introduced)

3.6 Post-test material properties

In Table 9 below, the final material characterisation test values, as well as values assumed for the modelling of the CL masonry, are reported.

Table 9 CL masonry characterisation test and numerical properties

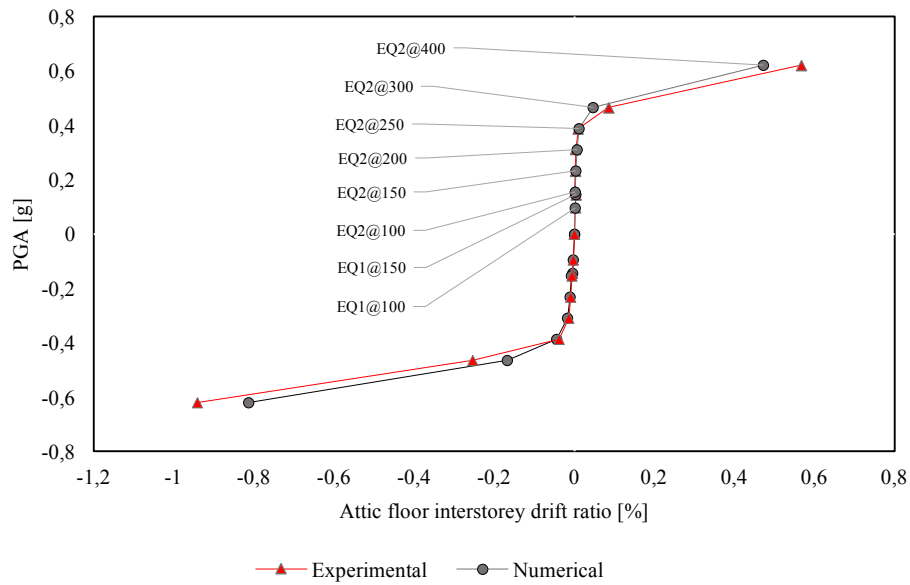
Symbol	Description	Test value ⁴	Employed value
ρ	Mass density [kg/m ³]	2101	1835
E	Masonry Young's modulus [MPa]	6519 ¹	---
E _{mo}	Mortar Young's modulus [MPa]	---	4607 ²
E _u	Unit Young's modulus [MPa]	---	7020 ²
ν	Poisson's ratio of masonry	---	0.25
f _m	Masonry compressive strength [MPa]	9.23	---
f _{mo}	Mortar compressive strength [MPa]	4.12	46.80
f _u	Brick compressive strength [MPa]	46.80	46.80
f _w	Flexural bond strength of mortar joints [MPa]	0.23	0.23
f _{v0}	Masonry (bed joint) initial shear strength (cohesion) [MPa]	0.26	0.26
μ	Masonry (bed joint) shear friction coefficient	0.55	0.55

¹ Secant stiffness to 10% f_m

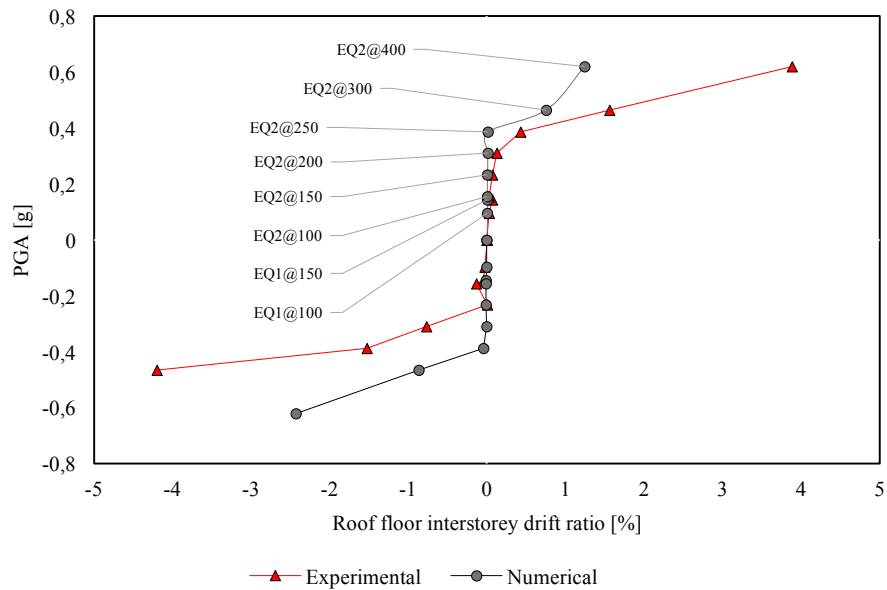
² Inferred by means of empirical formulae (Ciesielski 1999; ICBO 1991; Matysek and Janowski 1996; Brooks and Baker 1998)

3.7 Summary of results

The numerical outcomes obtained are summarised below, in the form of hysteresis envelope plots and deflected shape prior to collapse.

Figure 23 IDA: PGA vs attic floor IDR¹

¹ PGA vs. attic floor interstorey drift ratio (IDR) IDA curve plots the PGA [g] vs. the positive and negative direction IDR envelopes of attic floor [%] for each test.

Figure 24 IDA: PGA vs roof floor IDR¹

¹ PGA vs. roof interstorey drift ratio (IDR) IDA curve plots the PGA [g] vs. the positive and negative direction IDR envelopes of roof [%] for each test.

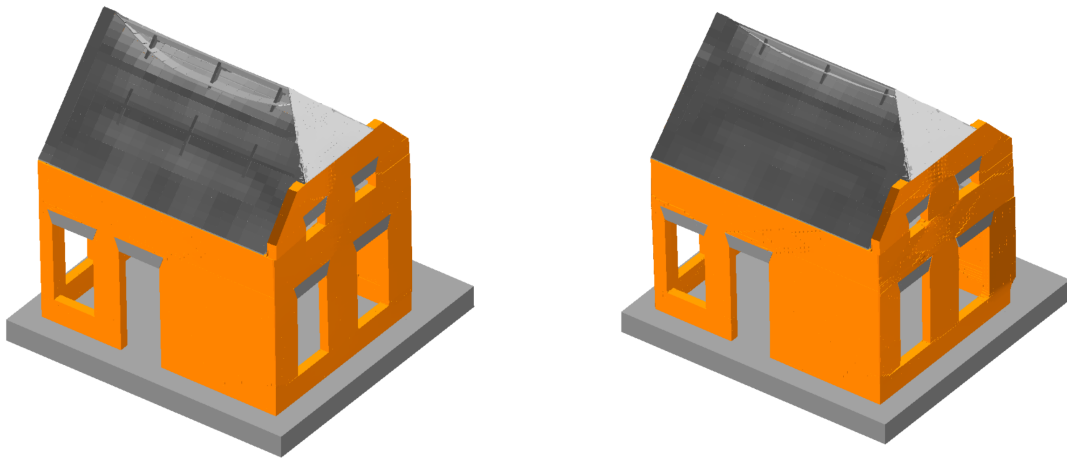


Figure 25 Deflected shapes (magnified x5) at maximum excursion prior to the end of test at EQ2@250 (left) and EQ2@300 (right)

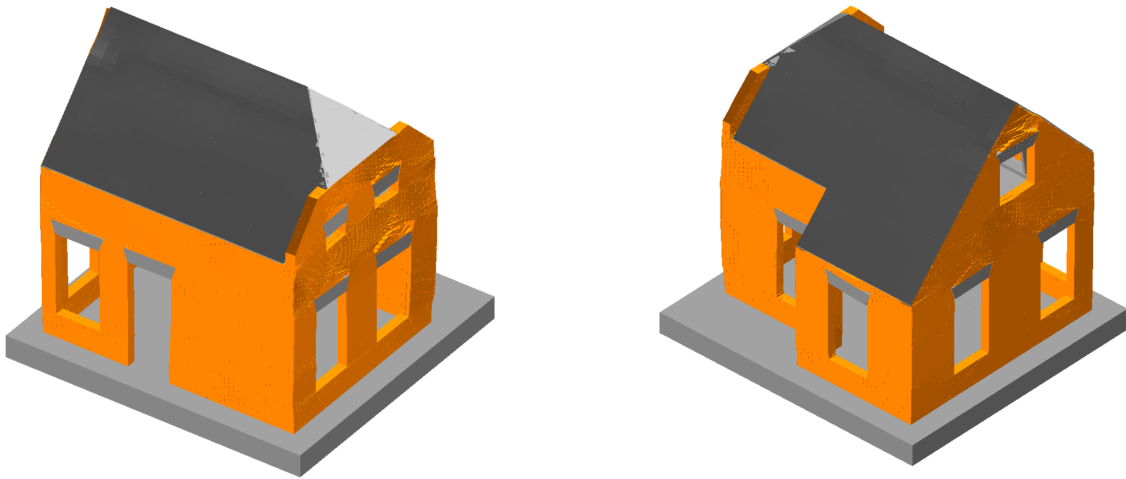
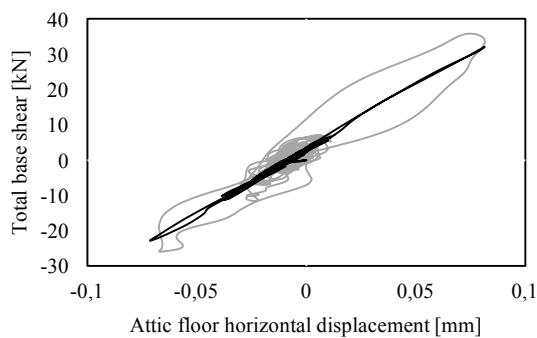


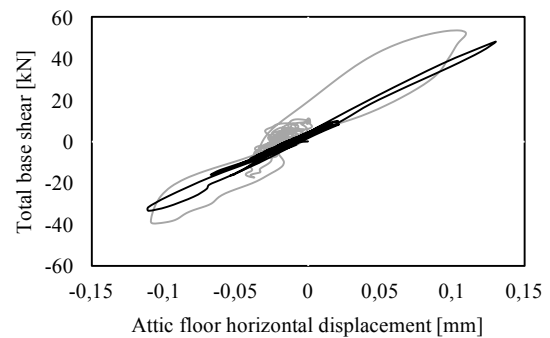
Figure 26 Gable out-of-plane mechanism, and damage of the South wall at EQ2@400 (magnified x2)

3.8 Floor hysteresis

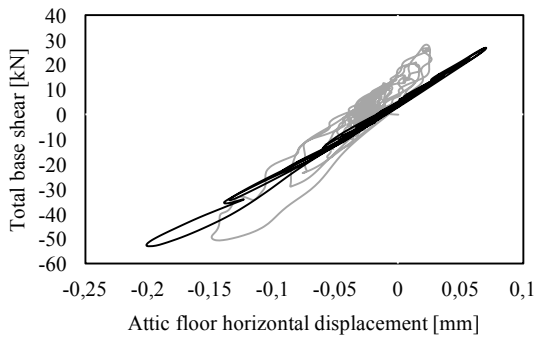
Floor hysteresis is defined as the total “base” shear [kN] vs. attic floor horizontal displacement relative to the base [mm]. Grey is experimental and black is numerical.



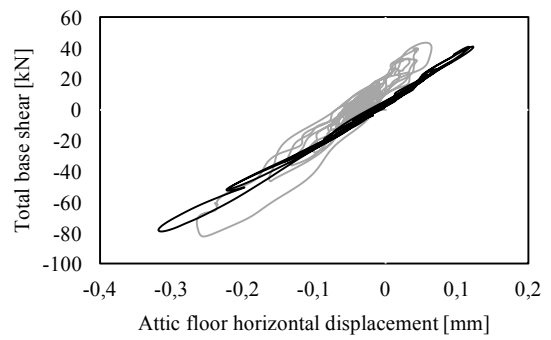
EQ1@100



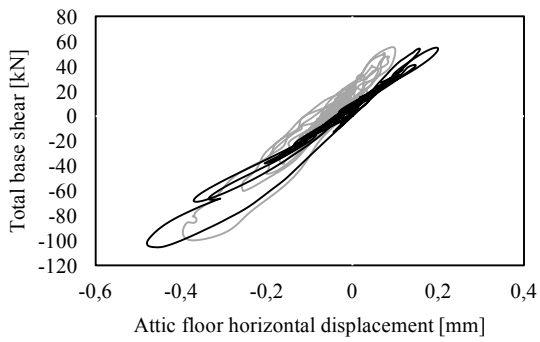
EQ1@150



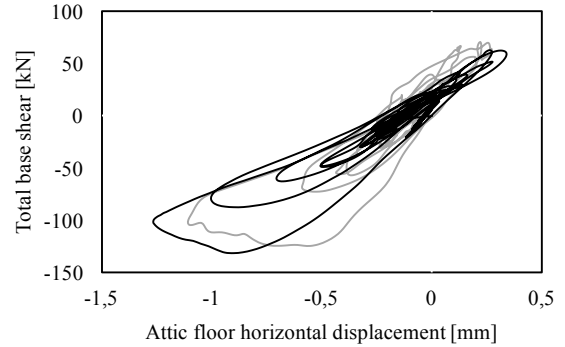
EQ2@100



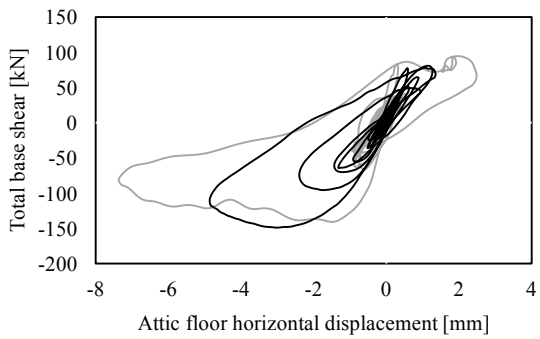
EQ2@150



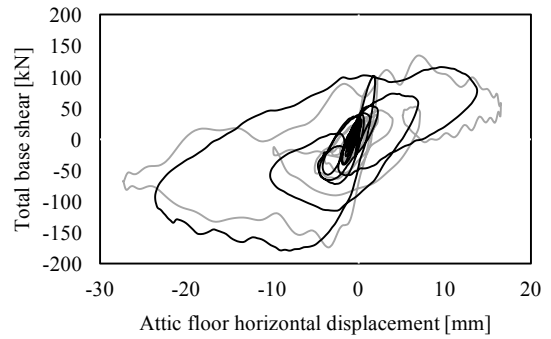
EQ2@200



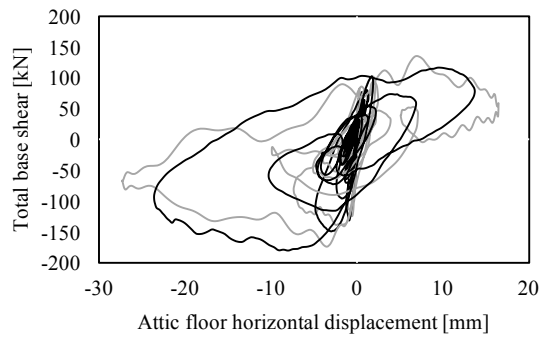
EQ2@250



EQ2@300



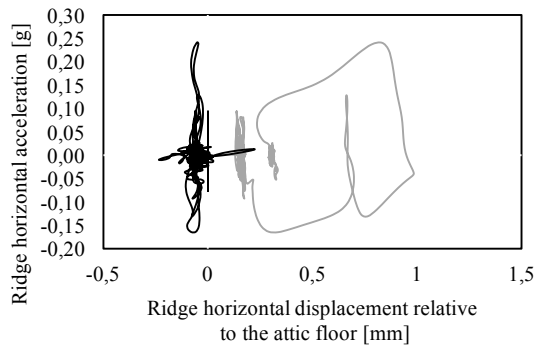
EQ2@400



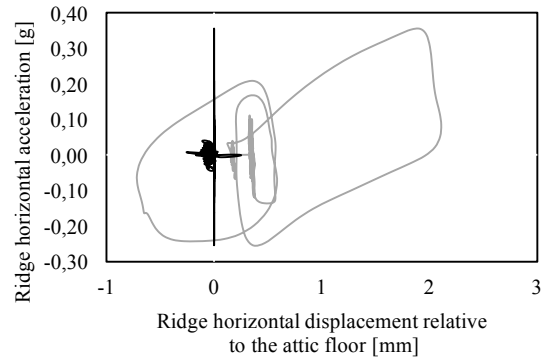
From EQ2@100 to EQ2@400

3.9 Roof acceleration hysteresis

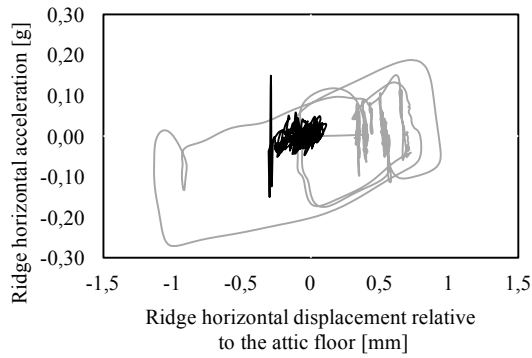
Roof acceleration hysteresis is defined as the ridge horizontal acceleration [g] vs. ridge horizontal displacement relative to the attic floor horizontal displacement [mm]. Grey is experimental and black is numerical.



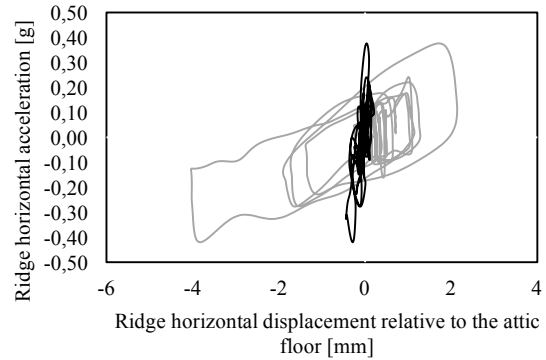
EQ1@100



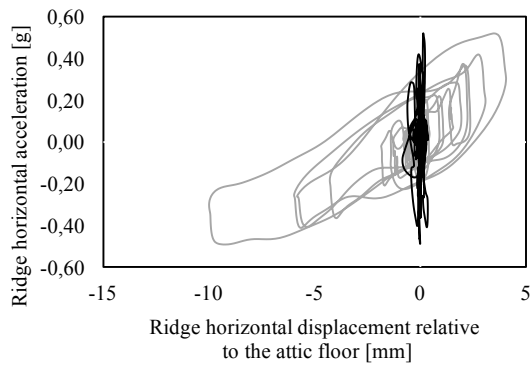
EQ1@150



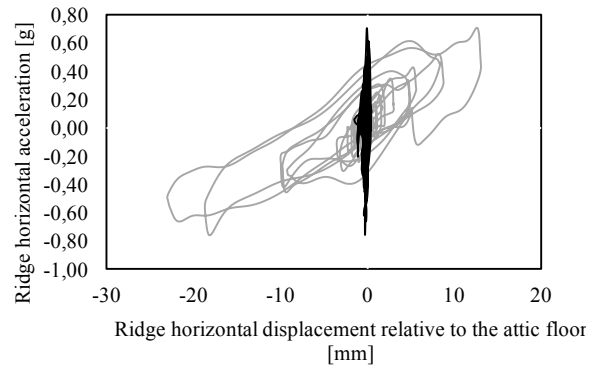
EQ2@100



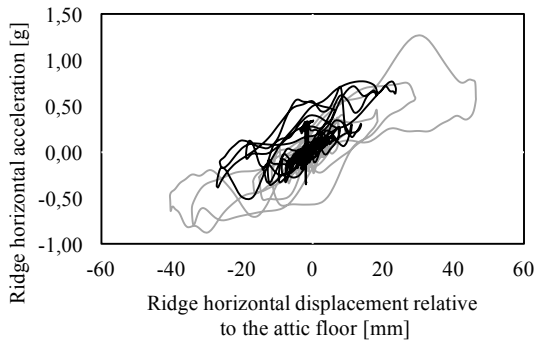
EQ2@150



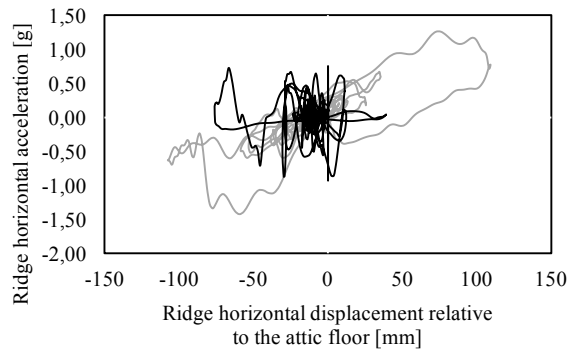
EQ2@200



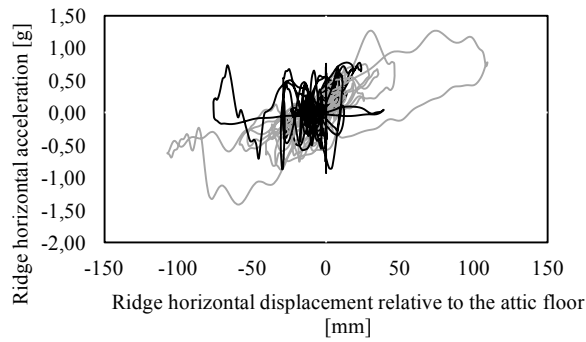
EQ2@250



EQ2@300



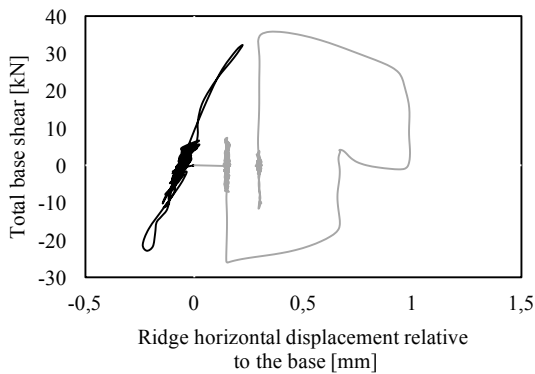
EQ2@400



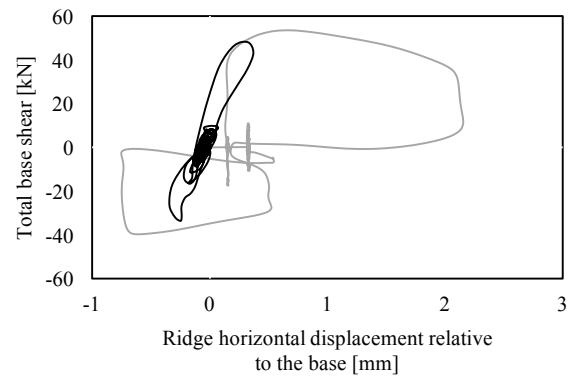
From EQ2@100 to EQ2@400

3.10 Global hysteresis

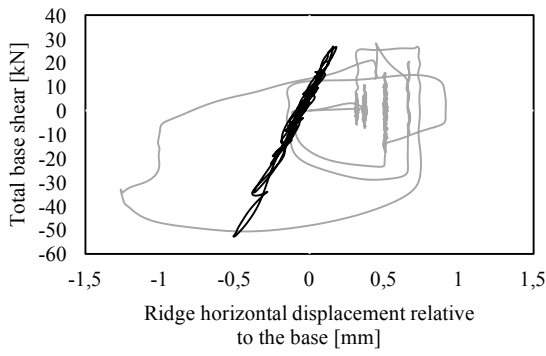
Global hysteresis is the total “base” shear [kN] vs. ridge hor. displacement relative to the base [mm]. Grey is experimental and black is numerical.



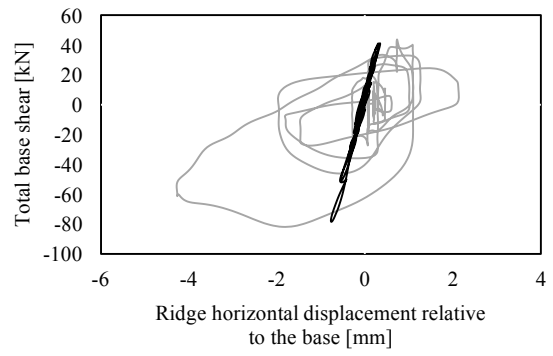
EQ1@100



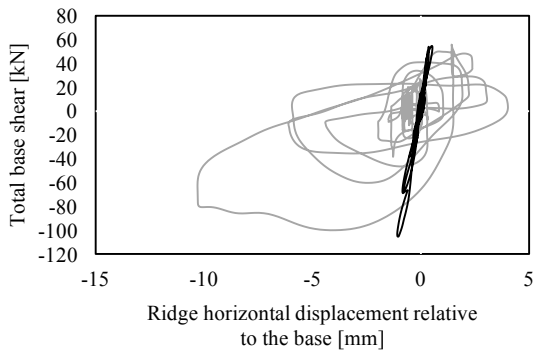
EQ1@150



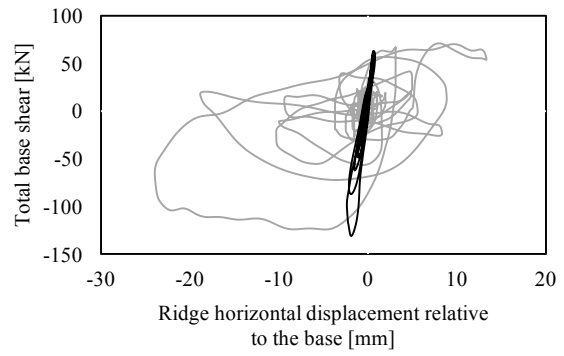
EQ2@100



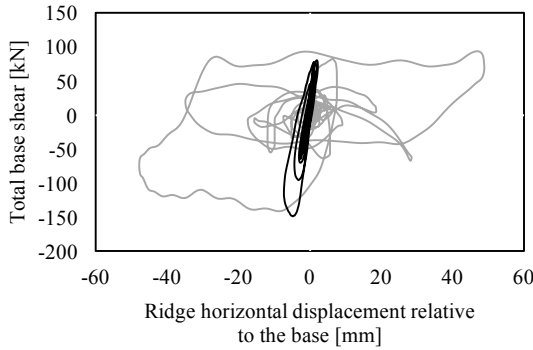
EQ2@150



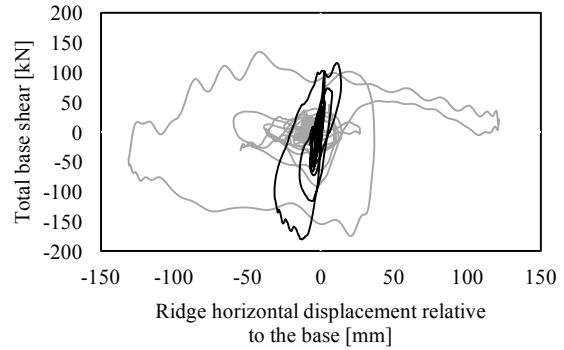
EQ2@200



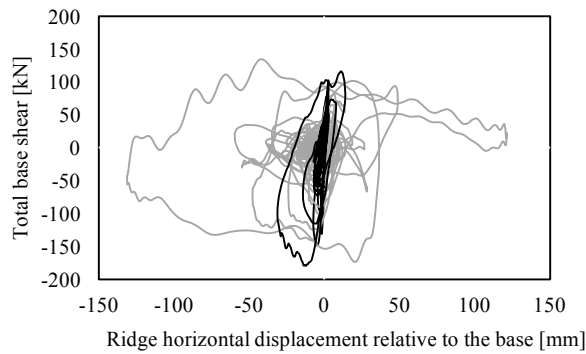
EQ2@250



EQ2@300



EQ2@400



From EQ1@100 to EQ2@400

3.11 Crack patterns and collapse mechanism

The final damage predictions for each wall are compared in this sub-section with their experimental counterpart (varied magnification).

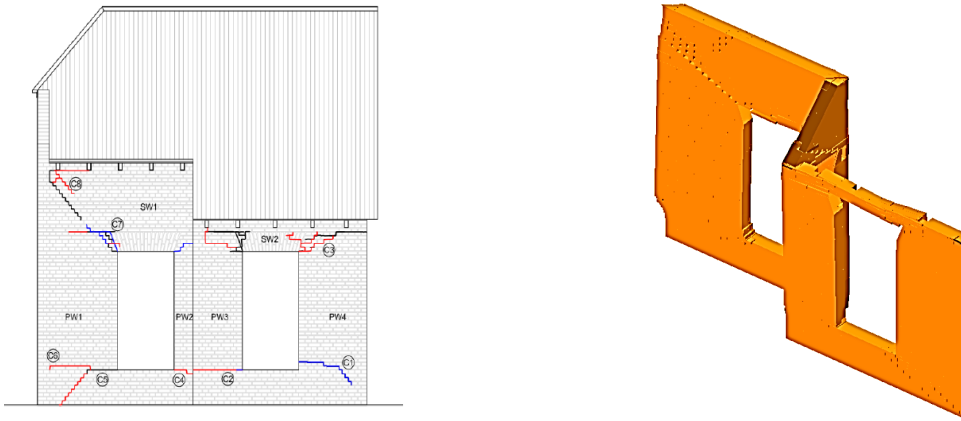


Figure 27 EQ2@300 _ Experimental (left) and numerical (right) damage plot of West wall

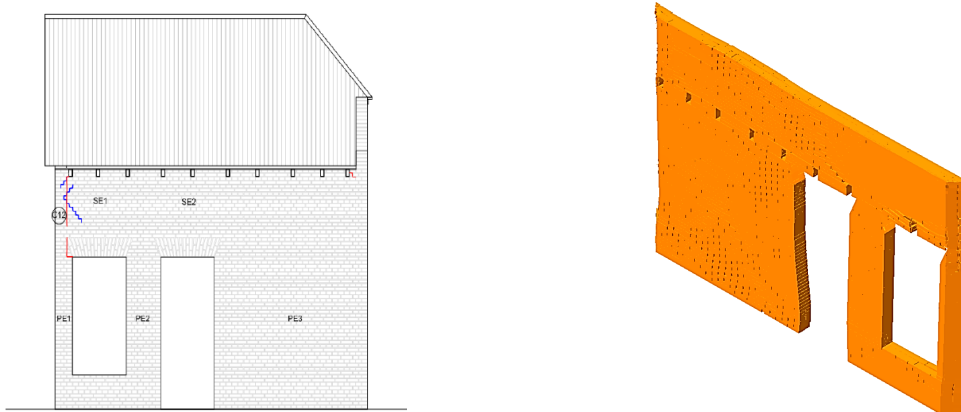


Figure 28 EQ2@300 _ Experimental (left) and numerical (right) damage plot of East wall

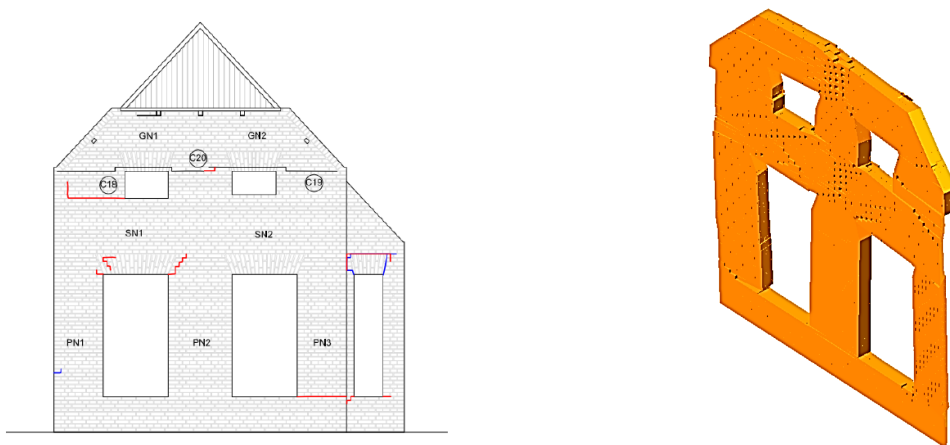


Figure 29 EQ2@300 _ Experimental (left) and numerical (right) damage plot of North wall



Figure 30 EQ2@300 _ Experimental (left) and numerical (right) damage plot of South wall



Figure 31 EQ2@400 _ Experimental (left) and numerical (right) damage plot of West wall

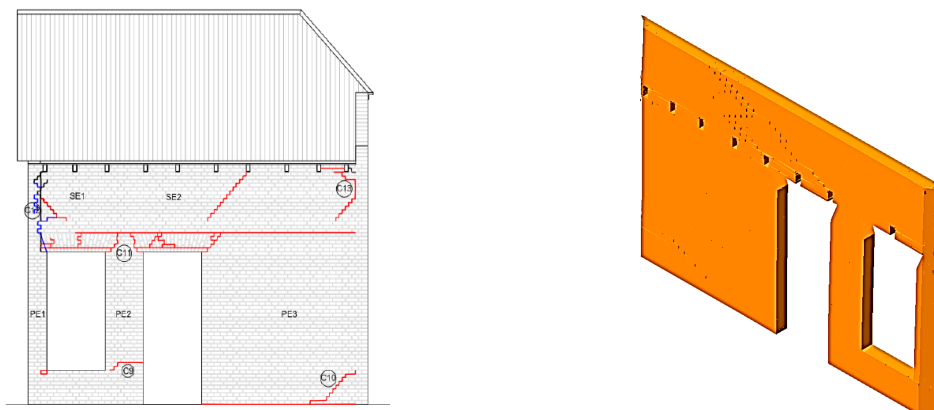


Figure 32 EQ2@400 _ Experimental (left) and numerical (right) damage plot of East wall

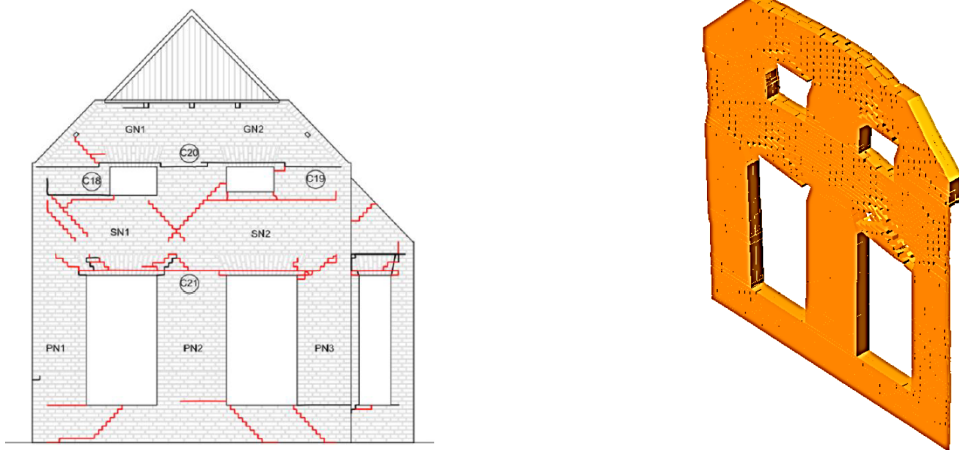


Figure 33 EQ2@400 _ Experimental (left) and numerical (right) damage plot of East wall

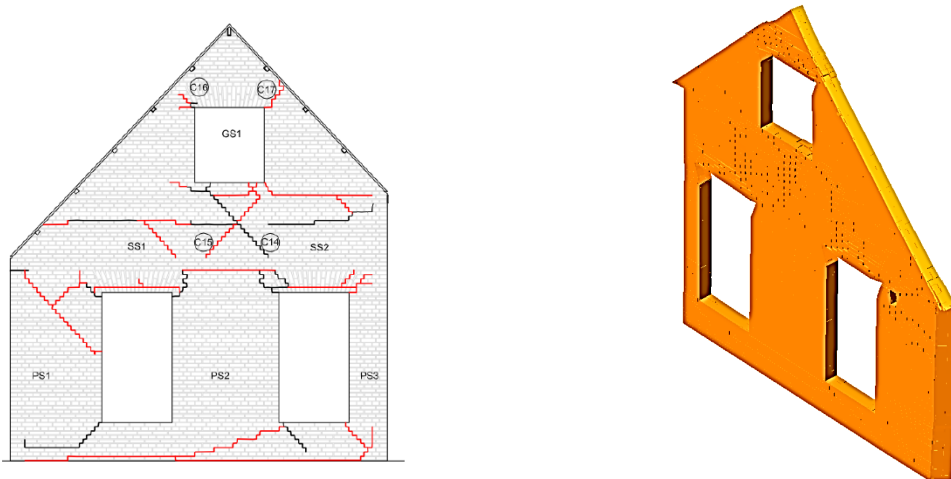


Figure 34 EQ2@400 _ Experimental (left) and numerical (right) damage plot of South wall

4 Closing Remarks

Two different full-scale URM house specimens subjected to earthquake loading were modelled using the Applied Element Method (AEM). This exercise confirmed the capability of the latter in analysing masonry structures under seismic excitation, independently of construction details and masonry material types.

For what concerns specimen EUC-BUILD1, the numerical results can be deemed as representative of the actual experimentally observed behaviour of the specimen. Indeed, the overall response was adequately captured, as also confirmed by comparing the numerical crack patterns of the last cycles with their experimental counterparts.

The numerical simulation of EUC-BUILD2 was slightly more challenging, due to the complexity of the roof structure. Indeed, the dynamic behaviour of the roof was well reproduced by the model only in the very last stages, thus leading to a numerical response that is stiffer than the experimentally recorded one.

The roof modelling strategy employed for EUC-BUILD1 differed slightly from that used for EUC-BUILD2. In the former, each plank was modelled separately, accounting both for nails slip, rigid rotation, flexural and shear deformation of the plank elements. The roof of EUC-BUILD2 was instead by means of an equivalent membrane element (Brignola et al., 2008) that intrinsically attempts to account for the abovementioned roof response components.

Further improvements regarding the latter approach are however currently under investigation, in particular for what concerns modelling of the connections between wooden elements (e.g. between beam/beam and beam/plank), since no specific experimental data are available.

Future modelling calibration efforts will also aim at trying to better capture the energy dissipation of EUC-BUILD2 specimen in first response cycles, through avenues such as e.g.:

- the possibility of adjusting, in the numerical model, the parameters that control degradation of cohesion and tensile strength (currently this is not possible, in the tool employed for these analyses);
- the feasibility of calibrating the equivalent viscous damping (currently this is not possible, in the tool employed for these analyses);
- meshing the bricks (so far modelled as rigid units), so that the energy dissipation associated to their deformation (in particular of CS bricks), cracking, splitting and crushing may be taken into account.

References

- ASI (2017) *Extreme Loading for Structures v5*, Applied Science International LLC., Durham (NC), USA.
- Brignola, A., Podestà, S., Pampanin, S. (2008) "In-plane stiffness of wooden floor" *Proceedings of the New Zealand Society for Earthquake Engineering Conference*, Wellington, New Zealand.
- Brooks J.J., Baker A. (1998) "Modulus of elasticity of masonry" *Masonry International*, Vol. 12, No. 2, pp. 58–63.
- Ciesielski R. (1999) "The dynamic module of elasticity of brick walls," *Proceedings of the Conference of the Committee of Civil Engineering PZITB*, Lublin, Poland.
- Graziotti F., Tomassetti U., Rossi A., Kallioras S., Mandirola M., Cenja E., Penna A., Magenes G. (2015a) "Full scale shaking table test on a URM cavity wall terraced house building" *Proceedings of the 16th World Conference on Earthquake Engineering*, Santiago, Chile.
- Graziotti F., Tomassetti U., Rossi A., Kallioras S., Mandirola M., Penna A., Magenes G. (2015b) "Experimental campaign on cavity-wall systems representative of the Groningen building stock," *Report n. EUC318/2015U*, European Centre for Training and Research in Earthquake Engineering (EUCENTRE), Pavia, Italy. Available from URL: <http://www.eucentre.it/nam-project>
- Graziotti F., Tomassetti U., Rossi A., Kallioras S., Mandirola M., Penna A., Magenes G. (2016) "Experimental campaign on a clay URM full-scale specimen representative of the Groningen building stock," *Report n. EUC128/2016U*, European Centre for Training and Research in Earthquake Engineering (EUCENTRE), Pavia, Italy. Available from URL: <http://www.eucentre.it/nam-project>
- ICBO (1991) *Uniform Building Code*, International Conference of Building Officials, USA.
- Kallioras S., Graziotti F., Tomassetti U., Marchesi B., Guerrini G., Penna A., Magenes G. (2017) "Experimental Seismic Performance of a Full-Scale Unreinforced Clay Masonry Building with Flexible Timber Diaphragms", Submitted to *Engineering & Structures*.
- Kim J.J., Reda Taha M. (2014) "Experimental and numerical evaluation of direct tension test for cylindrical concrete specimens," *Advances in Civil Engineering*, Vol. 2014, pp. 1-8.
- Malomo (2018) "Scrutinising the applicability of the Applied Element Modelling in the modelling of URM structures subjected to earthquake loading," *PhD Thesis*, University of Pavia, Italy. To be Submitted.
- Matysek P., Zbigniew J. (1996) "Analysis of factors affecting the modulus of elasticity of the walls," *Proceedings of the Conference of the Committee of Civil Engineering PZITB*, Lublin, Poland.
- Meguro K., Tagel-Din H. (2000) "Applied Element Method for structural analysis: Theory and application for linear materials," *JSCE International Journal of Structural Engineering and Earthquake Engineering*, Vol. 17, No. 1, pp. 21–35.
- Meguro K., Tagel-Din H. (2001) "Applied Element simulation of RC Structures under cyclic loading," *ASCE Journal of Structural Engineering*, Vol. 127, No. 11, pp. 1295-1305.
- Meguro K., Tagel-Din H. (2002) "Applied Element Method used for large displacement structure analysis," *Journal of Natural Disaster Science*, Vol. 24, No. 2, pp. 65-82.
- Mosayk (2016) "Using the Applied Element Method to model URM walls subjected to in-plane cyclic shear-compression," Pavia, Italy.

Appendix A – further details on URM model building in ELS

This Appendix is common to a series of reports by Mosayk (2017a, 2017b, 2017c) concerning the modelling of the shake-table testing of a number of URM full-scale specimens (EUC-BUILD1, EUC-BUILD2, LNEC-BUILD1 and LNEC-BUILD2), and aims at providing further details on the modelling of:

- Contact surfaces between elements (mortared or nailed)
- Timber planks (of slabs and roofs)
- Connectors, ties and steel anchors

In addition, the procedure to derive mortar elastic properties by means of homogenisation formulae is also reported.

A.1 AEM modelling of contact surfaces between elements

According to the AEM, the connection between rigid bodies is assured by interface springs. Each contact surface, indeed, is characterised by a user-defined number of springs in which both the material properties and the damping of the system are lumped.

The analysis accuracy is directly proportional to the number of springs as well as the mesh discretisation (i.e. the number of rigid bodies constituting the assembly). In most cases the default value of 25 springs per contact surface is sufficient to represent adequately the actual behaviour of a given structural elements both in static and dynamic range. However, when the numerical model requires a refined discretisation (i.e. a larger number of elements), then if the contact surface is sufficiently small, the amount of interface springs can be reduced consistently, so as to reduce the computation burden. In the analyses presented in this report, indeed, 9 springs per contact surface (of the discretised elements) were employed, given that this proved to constitute a good compromise between accuracy and computational demand.

As depicted in Figure A.1, the springs are located at specific contact points and distributed uniformly along the contact surfaces, representing the stress/strain state of a given volume DV (or DA in 2D), as well as the contact stiffness. This modelling approach thus readily allows assigning equivalent mechanical properties to the contacts in order to describe the actual behaviour of a wide range of connections between different elements (e.g. nailed, welded or interlocking connections).

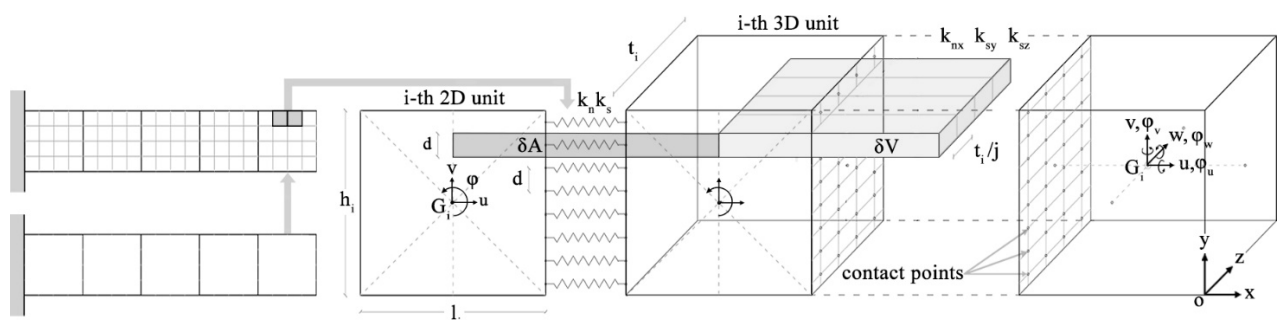


Figure A.1 Multi-scale discretization of both 2D and 3D rigid body assembly

In Figure A.2, below, the different types of contact connections considered in this modelling endeavour (which, it is reiterated, concerned the modelling of the shake-table testing of the four URM full-scale specimens listed above, not all of which are described in this one report) are shown.

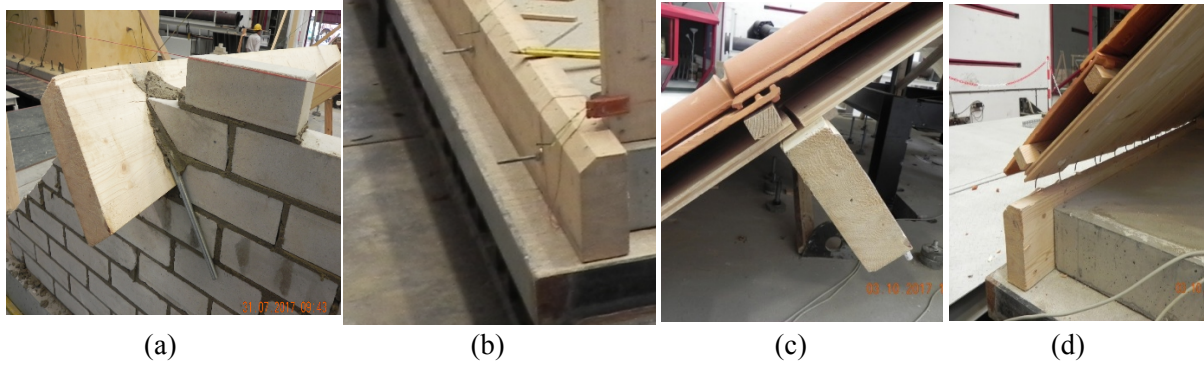


Figure A.2 L-shaped anchors (a), RC slab/beam connection (b), pure frictional contact between walls and planks (c) and nailed connections between boards and ridge/timber plate (d) (Correia et al., 2017)

A.1.1 Nailed connections between beam and plank elements

The mechanical connection between wooden boards and beams in traditional flexible diaphragms, is often provided by one or more steel nails distributed along the contact surface (Brignola et al., 2008) as reported in Figure A.3 below.

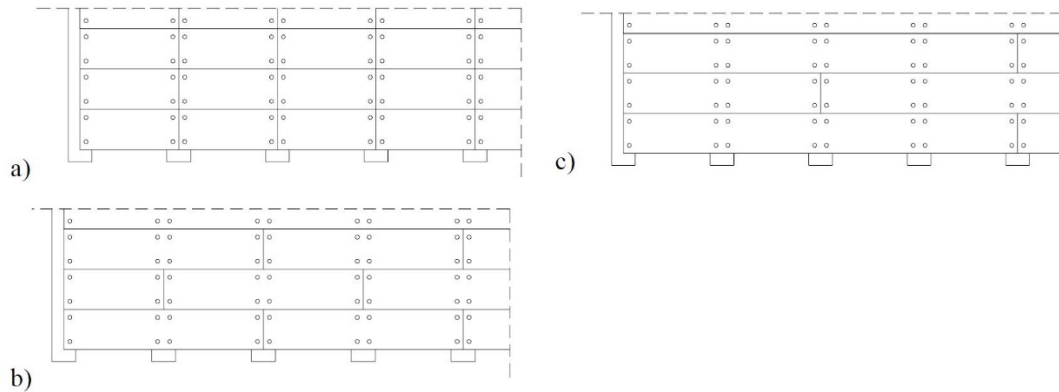


Figure A.3 Types of common nailed connections between beams and boards (Brignola et al., 2008)

The stiffness related to these interfaces are calibrated from the force-slip behaviour of the nail ($k_{ser} = F'/d'$), assuring the actual shear deformability to the connection. According to Eurocode 5 (2004), the slip modulus of a nail with diameter d' can be evaluated by means of Eq. (A.1) below, considering the simplified elastic-perfectly plastic response depicted in Figure A.4. Thus, considering a contact area A_c between board and beam, the following equivalent shear modulus Geq_{nails} , reported in Eq. (A.2) can be introduced and subsequently assigned to the related interface, where L represents the distance from the centroids of elements.

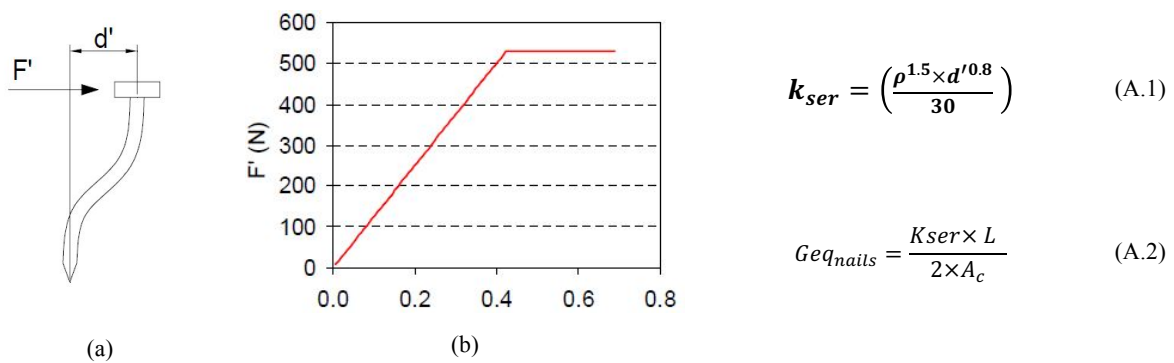


Figure A.4 Nail slip behaviour (a), and its force-displacement bilinear response (b) (Brignola et al., 2008)

With the aim of investigating the numerical response of this type of connection, several simplified models, of the type illustrated below in Figure A.5, were elaborated. In Table A.1 the main equivalent modelling parameters concerning the simplified model (compatible with the roof structure of both EUC-BUILD1, LNEC-BUILD1 and LNEC-BUILD2) are reported, whereas the associated force-displacement curve is depicted in Figure A.5(c).

Table A.1 Mechanical properties assigned to the simplified model

Simplified model subjected to pure shear loading conditions			
Material model	Bilinear material	Equivalent yield stress [MPa]	4
Beam height [mm]	220	Number of nails [-]	1
Board thickness [mm]	20	K_{ser} [N/mm]	965
Distance L between centroids [mm]	120	Yield force [N]	576
Area of contact [mm ²]	14400	Yield displacement [mm]	0.77
Nail diameter [mm ²]	4	$E_{eq,nail}$ [MPa]	11
Poisson coefficient [-]	0.25	$G_{eq,nail}$ [MPa]	4.4

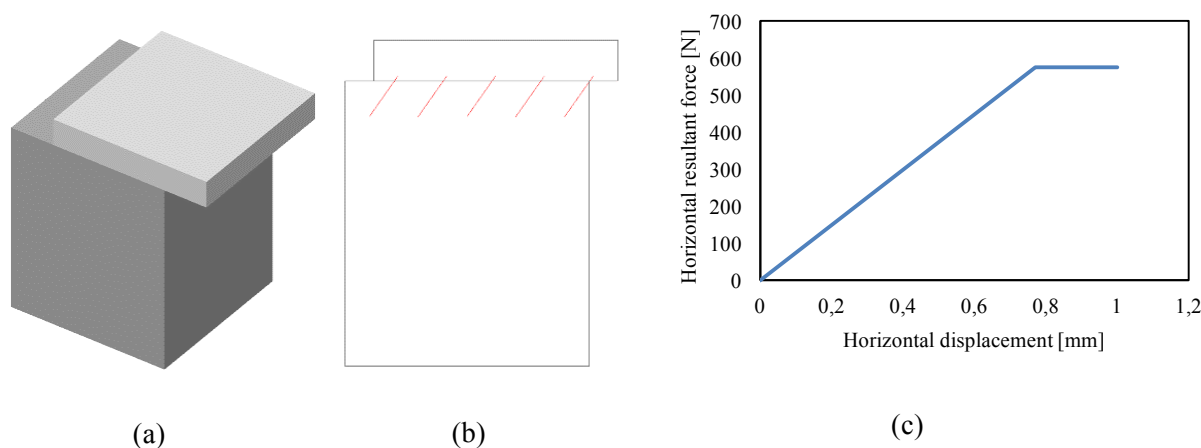


Figure A.5 Screenshot of the model (a), equivalent spring layer representing the nailed connection (b) and force-displacement plot (c)

In the abovementioned model, the base (beam) was fully fixed, whereas the upper element (plank) was free to move in the horizontal direction only. Hence, the interface springs were subjected to pure shear. With a view to account for the rotational deformability as well, the elastic modulus of the nail was inferred by multiplying $G_{eq,nail}$ by a factor of 2.5, yielding the typical constitutive equation for isotropic materials (Lekhnitskii, 1963).

However, further improvements related to the latter aspects are needed. Since the yield stress can be reached both in tension and in pure shear, the preliminary modelling results obtained for LNEC-BUILD1 using this methods prior the shake-table test, for instance, have shown that an early tensile failure of the connection (reached due to the increase in the rotation demand due to the relative displacement of adjacent boards) might occur.

Hence, small variations of this approach have been employed and applied for the subsequent models. For EUC-BUILD1, EUC-BUILD2, LNEC-BUILD1 and LNEC-BUILD2 (post-test refined simulations), indeed, the equivalent yield stress was increased consistently to avoid the early rotational failure of the beam-plank interface, as reported in Table A.2. This effectively rendered the updated contact surface as featuring an equivalent elastic interface, limited by the actual shear stiffness of the nail.

Table A.2 Mechanical properties of the nailed connection for EUC-BUILD2, LNEC-BUILD1 and LNEC-BUILD2

LNEC-BUILD1 (blind prediction model)			
Material model	Bilinear material	Equivalent yield stress [MPa]	4
Beam height [mm]	220	Number of nails [-]	2
Board thickness [mm]	20	K_{ser} [N/mm]	965
Distance L between centroids [mm]	120	Yield force [N]	---
Area of contact [mm ²]	14400	Yield displacement [mm]	---
Nail diameter [mm ²]	4	$E_{eq,nail}$ [MPa]	22
Poisson coefficient [-]	0.25	$G_{eq,nail}$ [MPa]	8.8
EUC-BUILD1, LNEC-BUILD1, LNEC-BUILD2 (post-test refined models)			
Material model	Bilinear material	Equivalent yield stress [MPa]	360
Beam height [mm]	220	Number of nails [-]	2
Board thickness [mm]	20	K_{ser} [N/mm]	965
Distance L between centroids [mm]	120	Yield force [N]	---
Area of contact [mm ²]	14400	Yield displacement [mm]	---
Nail diameter [mm ²]	4	$E_{eq,nail}$ [MPa]	22
Poisson coefficient [-]	0.25	$G_{eq,nail}$ [MPa]	8.8
EUC-BUILD2			
Material model	Bilinear material	Equivalent yield stress [MPa]	360
Beam height [mm]	180	Number of nails [-]	40 ¹
Board thickness [mm]	24	K_{ser} [N/mm]	965
Distance L between centroids [mm]	102	Yield force [N]	---
Area of contact [mm ²]	410000 ¹	Yield displacement [mm]	---
Nail diameter [mm ²]	4	$E_{eq,nail}$ [MPa]	13
Poisson coefficient [-]	0.25	$G_{eq,nail}$ [MPa]	5

¹ referred to the average contact area between a single transverse frame and the equivalent membrane element

A.1.2 Definition of “weak” and “cracked” mortar spring interfaces

In some cases (i.e. the modelling of EUC-BUILD1 and LNEC-BUILD1, post-test refined model) the connection between the lateral timber beam of the wooden roof structure, the RC slab and the URM cavity-wall system was characterised by peculiar mechanical properties. Indeed, the connection between the RC slab and the lateral timber beam of both EUC-BUILD1 and LNEC-BUILD1 consisted in a series of threaded bars (Graziotti et al., 2015), with the RC slab being then bonded to the transverse CS walls, while the beam is connected by means of a mortar layer to the CL brick masonry transverse walls.

Noteworthy, and also as gathered from Figure below, for both the specimens the gap between the RC slab and the longitudinal walls was filled after the temporary supports removal (i.e. after RC slab deflection); since the connection between these elements was provided only by this mortar layer, a “weak” spring interface was adopted, with a very low flexural and shear stiffness.

Further, in the case of LNEC-BUILD1, with aim to take into account the damage occurred at the interface between the RC slab and the lateral during transportation phases (Tomassetti et al., 2017), a “cracked” mortar spring interface has been introduced. This layer has almost zero flexural and shear stiffness, zero tensile and shear strength, and a compressive strength equal to the one of the brick.



Figure A.6 Constructional details of the gap between CL walls/timber beam (a) and CS walls/RC slab (b) (Graziotti et al., 2015)

A.2 Numerical modelling of plank elements

The overall diaphragm flexibility can be evaluated by analysing the contribution to the in-plane deformation of the timber floor separately, as suggested by Brignola et al. (2008). In this sense, three different deformability contributions are distinguished: the flexural deformation of the single board, shear deformation of the single board and the rigid rotation of the board due to nails slip (see Figure A.7).

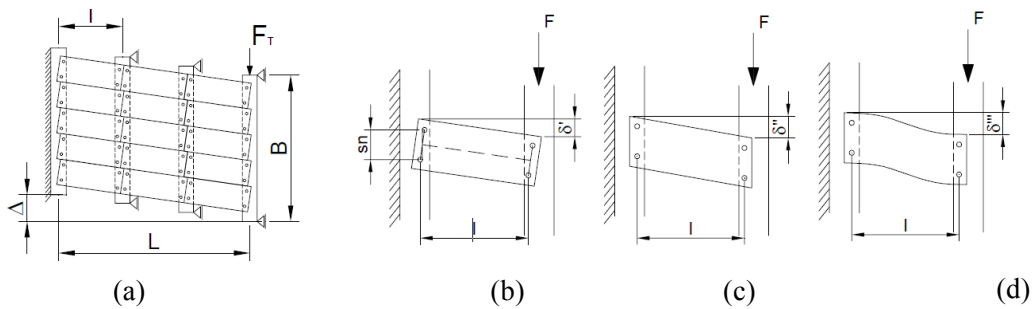


Figure A.7 Deformability contributions of a given flexible diaphragm (Brignola et al., 2008)

Thus, it is possible to define an equivalent shear modulus that combines the three contributions of flexibility according to Eq. (A.3), where X is the shear factor, G shear modulus of planks, E flexural modulus parallel to grain of planks, A board section, I moment of inertia of plank section and s_n is the wheelbase between beams. Moreover, this result obtained for one board can be extended to the whole diaphragm when the wood planks are interrupted at each beams, as noted by Brignola et al. (2008).

$$Geq_{plank} = \left(\frac{X}{A}\right) \left(\frac{l}{k_{ser} s_n^2} + \frac{X}{GA} + \frac{L}{12EI}\right)^{-1} \quad (A.3)$$

However, since the deformability of nails is already accounted by the spring interface described in the previous sub-section, Eq. (A.4) can be simplified as follows:

$$Geq_{plank} = \left(\frac{X}{A}\right) \left(\frac{X}{GA} + \frac{L}{12EI}\right)^{-1} \quad (A.4)$$

Two main modelling strategies have been employed for modelling the roof structures of the URM full-scale specimens mentioned above, due to different construction details. Indeed, the roof of EUC-BUILD1, LNEC-BUILD1 and LNEC-BUILD2 was a relatively simple bearing system,

constituted by longitudinal beams covered by transverse boards and tiles (see Figure A.8). The roof of EUC-BUILD2, instead, was formed by a series of wooden frames supporting the planks and tiles assembly. Furthermore, the gable structure required specific constructional details, as described in the related report (Graziotti et al., 2016).

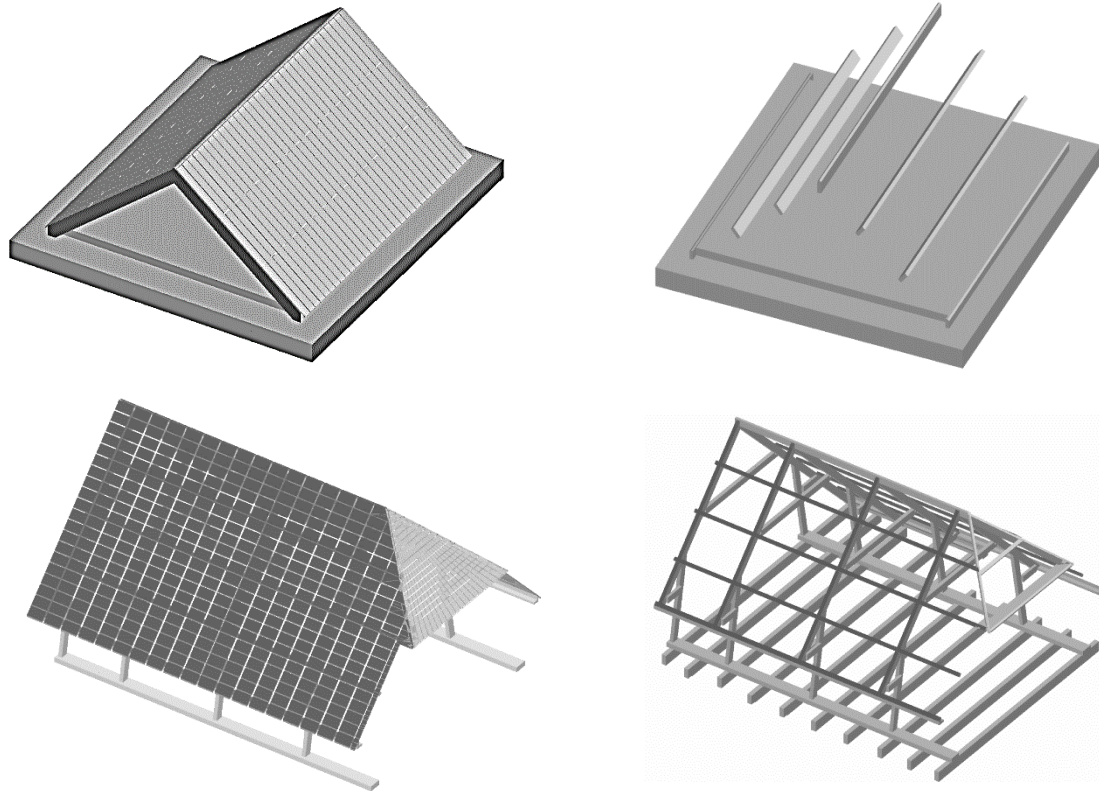


Figure A.8 Roof structure of LNEC-BUILD2 (above) and EUC-BUILD2 (below)

Hence, in case of EUC-BUILD1, LNEC-BUILD1 and LNEC-BUILD2 each plank was modelled separately, resulting in a more accurate numerical response, whereas the planks of EUC-BUILD2 were modelled as an equivalent continuous membrane with the aim of reducing the computational burden and the modelling efforts. The latter approach, as it is clearly observable from the results shown in the corresponding report, still requires further enhancements.

In Table A.3, the main numerical parameters, inferred using Eq. (A.4) and subsequently employed for the modelling of the abovementioned full-scale specimens, are briefly summarised:

Table A.3 Plank material properties employed for the modelling of for EUC-BUILD2, LNEC-BUILD1 and LNEC-BUILD2

LNEC-BUILD1 (blind prediction model)			
Geometrical parameters		Inferred values	
Board thickness	20 mm	Shear factor	1.2
Board width	180 mm	Shear deformation of the single board	8e-07 m/N
Elastic modulus of wood	12000 MPa	Deformability due to rigid rotation of the board	5.18e-0.5 m/N
Shear modulus of wood	750 MPa	Flexural deformation of the single board	4.16e-06 m/N
Board Length	1.8 m	Equivalent shear modulus $G_{eq,plank}$	120.80 MPa
EUC-BUILD1, LNEC-BUILD1, LNEC-BUILD2 (post-test refined models)			
Board thickness	20 mm	Shear factor	1.2
Board width	180 mm	Shear deformation of the single board	8e-07 m/N

Elastic modulus of wood	12000 MPa	Deformability due to rigid rotation of the board	5.18e-05 m/N
Shear modulus of wood	750 MPa	Flexural deformation of the single board	4.16e-06 m/N
Board Length	1.8 m	Equivalent shear modulus Geq_{plank}	120.80 MPa
EUC-BUILD2			
Board thickness	18 mm	Shear factor	1.2
Board width	150 mm	Shear deformation of the single board	2.67e-06 m/N
Elastic modulus of wood	5000 MPa	Deformability due to rigid rotation of the board	7.43e-05 m/N
Shear modulus of wood	333 MPa	Flexural deformation of the single board	2.63e-05 m/N
Board Length	2.0 m	Equivalent shear modulus Geq_{plank}	22.98 MPa

A.3 Connectors, ties and steel anchors elements

The use of metal reinforcements and connectors, such as ties and L-shaped anchors (see Figure A.9), is a relatively common practice in the construction of URM buildings in the Groningen area. These elements, as confirmed also by experimental tests on structural sub-components (Graziotti et al., 2015), strongly affect the behaviour of URM constructions. In Figure A.10 the modelling of the ties elements and the L-shaped steel anchors for EUC-BUILD1 and LNEC-BUILD1 is shown.

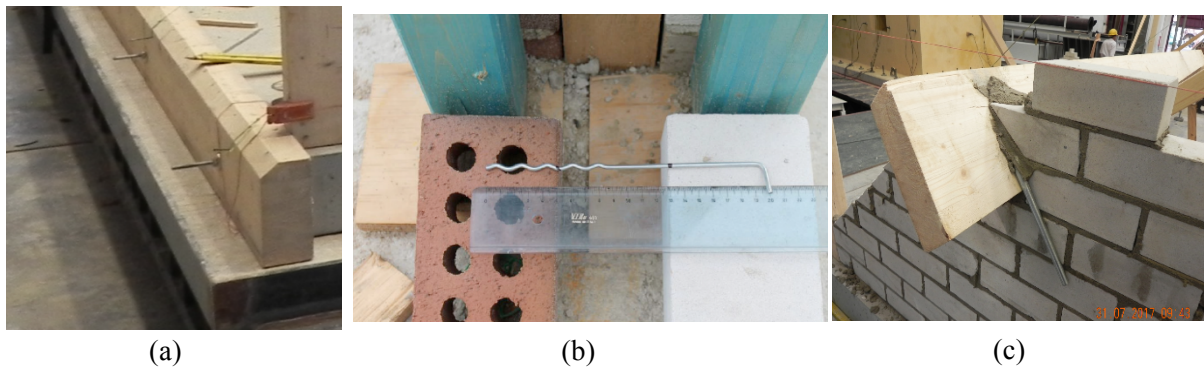


Figure A.9 RC slab/beam connection (a), steel ties (b) and L-shaped anchors (c) (Correia et al., 2017)

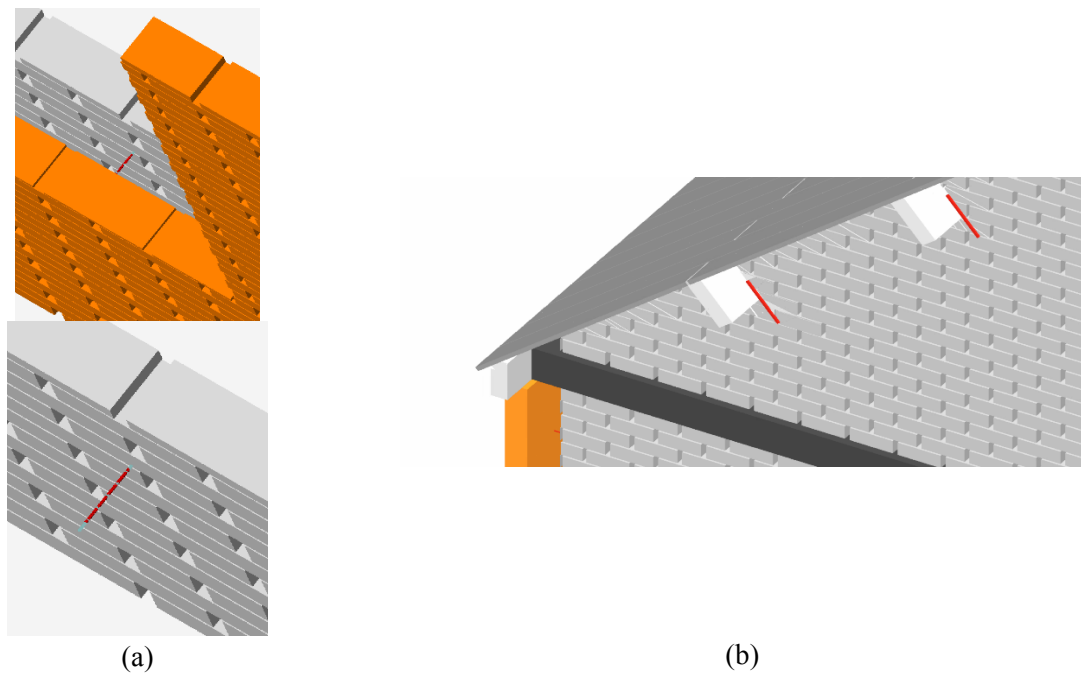


Figure A.10 Nails connections of EUC-BUILD1 (a) and L-shaped anchors of LNEC-BUILD1 (b)

As mentioned above, the connectors between the RC slab and the lateral timber beams were made of threaded bars (diameter of 10 mm). The steel ties connecting the CS to the CL brick masonry walls were instead characterised by a diameter of 3.4 mm, whereas the L-shaped steel anchors (diameter of 15 mm) assured the connection between the timber beam extremities and the gables.

The RC slab/lateral timber beam connector was modelled as an equivalent elastic spring interface, avoiding spurious relative displacement not observed during the tests, whereas both the L-shaped anchors and the ties were modelled by means of three-dimensional beam elements.

In Table A.4, the constitutive models and the most relevant mechanical properties are briefly summarised:

Table A.4 Constitutive models and mechanical properties of metal connectors and anchors

EUC-BUILD1, LNEC-BUILD1, LNEC-BUILD2			
RC slab/lateral timber beams		L-shaped anchors and steel ties	
Material model	Elastic material	Material model	Bilinear material
Element type	Spring interface	Element type	3D girder
Young's modulus [MPa]	10000	Young's modulus [MPa]	210000
Shear modulus [MPa]	400	Shear modulus [MPa]	84000
Friction coefficient [-]	0.4	Friction coefficient [-]	0.8
Separation strain [-]	1e+08	Separation strain [-]	100

A.4 Derivation of mortar Young's modulus from homogenisation formulae

As extensively discussed in Mosayk (2016), since the Young's modulus for both the masonry panels assembly and the bricks are known (from material characterisation tests), the Young's modulus of the mortar can be computed by means of the equations reported in Table A.5, often employed to develop a homogenisation process (i.e. to estimate the Young's modulus of a masonry panel when in knowledge of the Young's moduli of its brick and mortar components).

All four equations described below, where ξ is the ratio of brick's height to the thickness of mortar joint, were used to infer E_{mo} , and then the ensuing average considered for the models. It is noted that when unrealistic values were obtained from a given equation, such values were not considered in computation of the average value.

Furthermore, it is noted that the shear modulus G_{mo} was obtained assuming $G = E/(2(1 + \nu)) = 0.4E$ with $\nu = 0.25$, because no experimental data concerning this specific parameter was available.

Table A.5 Derivation of the Young's modulus of mortar through homogenization criteria

Reference	Homogenisation formulae		Reference	Homogenisation formulae	
Brooks et al. (1998)	$E_{mo} = \left(\frac{-4E_m E_b}{25E_m - 29E_b} \right)$	(A.5)	Matysek et al. (1996)	$E_{mo} = \left(\frac{E_m E_b}{E_b - 1.25\xi(E_m - E_b)} \right)$	(A.6)
Ciesielski (1999)	$E_{mo} = \left(\frac{-E_m E_b}{5E_m - 6E_b} \right)$	(A.7)	ICBO (1991)	$E_{mo} = \left(\frac{E_m E_b}{\xi(E_m - E_b) + E_b} \right)$	(A.8)

In the following Table A.6, the mortar Young's moduli and the mean values subsequently adopted for the modelling of the full-scale URM specimens are reported.

Table A.6 Mortar Young's modulus calculation for each full-scale specimen

LNEC-BUILD1 (blind prediction model)			
CS			
Reference	E_{mo} [MPa]	Reference	E_{mo} [MPa]
Brooks et al. (1998)	895	Matysek et al. (1996)	675
Ciesielski (1999)	1060	ICBO (1991)	1360
Mean value [MPa]			
997			
CL			
Reference	E_{mo} [MPa]	Reference	E_{mo} [MPa]
Brooks et al. (1998)	2927	Matysek et al. (1996)	2927
Ciesielski (1999)	3261	ICBO (1991)	Not reliable
Mean value [MPa]			
3039			
LNEC-BUILD1, LNEC-BUILD2 (post-test refined models)			
CS			
Reference	E_{mo} [MPa]	Reference	E_{mo} [MPa]
Brooks et al. (1998)	4626	Matysek et al. (1996)	3935
Ciesielski (1999)	5059	ICBO (1991)	Not reliable
Mean value [MPa]			
4537			
CL			
Reference	E_{mo} [MPa]	Reference	E_{mo} [MPa]
Brooks et al. (1998)	3184	Matysek et al. (1996)	3184
Ciesielski (1999)	4237	ICBO (1991)	Not reliable
Mean value [MPa]			
3039			
EUC-BUILD1			
CS			
Reference	E_{mo} [MPa]	Reference	E_{mo} [MPa]
Brooks et al. (1998)	4626	Matysek et al. (1996)	3935
Ciesielski (1999)	5059	ICBO (1991)	Not reliable
Mean value [MPa]			
4537			
CL			
Reference	E_{mo} [MPa]	Reference	E_{mo} [MPa]
Brooks et al. (1998)	Not reliable	Matysek et al. (1996)	Not reliable
Ciesielski (1999)	Not reliable	ICBO (1991)	Not reliable
Adopted value [MPa]			
4537 (equal to the one of the CS mortar)			
EUC-BUILD2			
CL			
Reference	E_{mo} [MPa]	Reference	E_{mo} [MPa]
Brooks et al. (1998)	4508	Matysek et al. (1996)	4508
Ciesielski (1999)	4805	ICBO (1991)	Not reliable
Mean value [MPa]			
4607			

A.5 References

- Brignola, A., Podestà, S., Pampanin, S. (2008) "In-plane stiffness of wooden floor" *Proceedings of the New Zealand Society for Earthquake Engineering Conference*, Wellington, New Zealand.
- Eurocode 5, "Design of timber structures", EN 1995-1-1 (2004)
- Graziotti F., Tomassetti U., Rossi A., Kallioras S., Mandirola M., Cenja E., Penna A., Magenes G. (2015) "Experimental campaign on cavity-wall systems representative of the Groningen building stock," *Report n. EUC318/2015U*, European Centre for Training and Research in Earthquake Engineering (EUCENTRE), Pavia, Italy. Available from URL:
- Graziotti F., Tomassetti U., Rossi A., Kallioras S., Mandirola M., Penna A., Magenes G. (2016) "Experimental campaign on a clay URM full-scale specimen representative of the Groningen building stock," *Report n. EUC128/2016U*, European Centre for Training and Research in Earthquake Engineering (EUCENTRE), Pavia, Italy. Available from URL: <http://www.eucentre.it/nam-project>
- Lekhnitskii S.G., Fern P. (1964) "Theory of Elasticity of an Anisotropic Elastic Body," *Physics Today*, Vol. 17, No. 1, p. 84.
- Mosayk (2016) "Using the Applied Element Method to model URM walls subjected to in-plane cyclic shear-compression," Pavia, Italy.
- Mosayk (2017a) "Using the Applied Element Method to model the shake-table testing of two full-scale URM houses," Pavia, Italy.
- Mosayk (2017b) "Using the Applied Element Method to model the collapse shake-table testing of a URM cavity wall structure," Pavia, Italy.
- Mosayk (2017c) "Using the Applied Element Method to model the collapse shake-table testing of a terraced house roof substructure," Pavia, Italy.
- Tomassetti U., Kallioras S., Graziotti F., Correia A. (2017b) "Final report on the construction of the building prototype at the LNEC laboratory," European Centre for Training and Research in Earthquake Engineering (EUCENTRE), Pavia, Italy.